UNIVERSITY
OF WARMIA AND MAZURY
IN OLSZTYN

The process of alkaline water electrolysis for the production of ultra-pure hydrogen and oxygen gases for PEM fuel cells´ applications

by

Mateusz Łuba, M.Sc.

A thesis presented to the University of Warmia and Mazury in Olsztyn in partial fulfilment of the requirements for the degree of

DOCTORATE IN PHILOSOPHY

Engineering and Technology

This work was written at the Department of Chemistry UWM in Olsztyn, under the supervision of Professor Bogusław Pierożyński, D.Sc., Ph.D., M.Eng. and Associate Professor Piotr Sołowiej, D.Sc., Ph.D., M.Eng.

© University of Warmia and Mazury in Olsztyn 2022

UNIWERSYTET
WARMIŃSKO-MAZURSKI
W OLSZTYNIE

Proces elektrolizy wody w układzie alkalicznym na potrzeby produkcji ultra-czystego wodoru i tlenu do zastosowania w ogniwach paliwowych typu PEM

wykonana przez

mgr Mateusza Łubę

Praca dyplomowa została wykonana w Uniwersytecie Warmińsko-Mazurskim w Olsztynie, która stanowi częściową realizację wymagań do uzyskania stopnia

DOKTORA NAUK INŻYNIERYJNO-TECHNICZNYCH

Rozprawa doktorska wykonana w Katedrze Chemii UWM pod kierunkiem
prof. dr hab. inż. Bogusława Pierożyńskiego oraz
dr hab. inż. Piotra Sołowieja, prof. UWM

© Uniwersytet Warmińsko-Mazurski w Olsztynie 2022

Table of Contents

1. Abstract 4
2. Streszczenie 7
3. Introduction 11
   3.1. The importance of alkaline water electrolysis for the world's energy sector 11
   3.2. The mechanisms of HER and OER half-reaction 13
4. Work Objectives 15
5. Materials and Methods 16
   5.1. Employed Techniques 16
   5.2. Supporting Electrolytes, Base Catalytic Material and its Modifications 19
6. Results and Discussion 21
   6.1. Hydrogen Evolution Reaction 21
   6.2. Oxygen Evolution Reaction 29
   6.3. Alkaline Water Electrolyser Unit 41
7. Conclusions 51

Future Perspectives 52
References 53
List of Tables and Figures 58
List of Abbreviations and Symbols 60
Monothematic List of Publications as the Basis for the Ph.D. Thesis 61
Scientific Achievements 62
Scientific Conferences: 64
External Internship: 65
Bibliometric Data (Scopus): 66
Acknowledgments 66

1. Abstract

The key aim of research activities covered by this doctoral dissertation was to develop cost effective and durable under long-term operation, advanced Ni foam-based electrocatalyst materials, as highly effective cathode and anode electrodes for hydrogen evolution (HER) and oxygen evolution (OER) reactions, respectively. In addition to their long-term durability, highly efficient electrode materials should primarily be characterized by low overpotential values for the corresponding electrochemical processes. It is commonly known that the process of water splitting is driven above the thermodynamic requirement of 1.229 V. Moreover, the catalyst substrates should not only be based on materials that are abundant in natural environment, but they should also be characterized by high electrical conductivity and extended, electrochemically active surface area.

Thus, in the first part of this work, a comprehensive study on the kinetics of the HER cathodic process is presented. The HER was examined at innovative, composite catalyst materials, such as: *as received* nickel foam (Ni foam) and Ni foam base material modified with very small amounts of iridium nanoparticles. Two methods of metal deposition were implemented here, i.e. spontaneous and electrochemical surface deposition. All electrochemical examinations were performed in a three-compartment, pyrex glass-made electrochemical cell in 0.1 M NaOH electrolyte solution, prepared by means of a Direct-Q3 UV ultra-pure water purification system from Millipore (18.2 MΩ cm water resistivity), at room temperature. Electrochemical impedance spectroscopy and *quasi* steady-state polarization methods were employed through the operation of the *Solatron 12,608* W Full Electrochemical System, consisting of 1260 Frequency Response Analyzer (FRA) and 1287 Electrochemical Interface (EI). In addition, spectroscopic characterization of catalyst materials was performed by means of SEM/EDX (Scanning Electron Microscopy/Energy-Dispersive X-Ray Spectroscopy) analyses.

Based on the recorded charge-transfer resistance, exchange current-density, interfacial capacitance and other parameters, it was reported that very low amounts of Ir deposit on the surface of pre-treated Ni foam materials caused a radical enhancement of their HER catalytic activity. The obtained results clearly indicated significant opportunities for the Ir nanoparticle-modified Ni foam composites towards the HER process and their possible employment in commercial, alkaline water electrolysers.

The effectiveness of complex water splitting process depends on the kinetics of both the HER and OER electrode reactions. While the cathodic hydrogen evolution is characterized by relatively low overpotential values, the OER remains a major factor that controls the overall rate of water decomposition process. Therefore, the second part of this thesis is concerned with the OER reaction's kinetics. The latter was also examined on the catalytically modified Ni foam materials. Hence, small amounts of platinum, freshly prepared transition metal-based electrocatalysts (cobalt and molybdenum) and extensively electrooxidized Ni foam electrodes were selected as anodes. Interestingly, the OER catalysts prepared based on non-noble metals proved to be beneficial, when compared to both the Pt-modified and electrooxidized Ni foam electrodes, which exhibited inferior OER electrochemical activity.

In the last part of this work, practical examinations of alkaline water electrolysis were carried-out by means of an innovative, 500 W laboratory size AWE (Alkaline Water Electrolyser) system, equipped with Pd-activated Ni foam or unmodified Ni foam cathodes, and *in situ* electrooxidized Ni foam anodes. The total catalytic activity and stability tests (dc. galvanostatic and ac. impedance measurements) of the proposed AWE system were carried-out by means of the *Solatron 12,608* W Full Electrochemical System and 30 V/30 A dc. power supply unit (PeakTech®). On the other hand, during the H_2O electrolysis process, samples of O_2 and H_2 gases were collected and analyzed with the use of a gas chromatograph (GC) Shimadzu GC2014 model, equipped with a chromatographic column and a helium detector with

pulse discharge (PD-HID-Pulsed Discharge Helium Ionization Detector). It was reported that the AWE system equipped with the unmodified Ni foam cathodes (in combination with surface-electrooxidized Ni foam anodes) achieved a maximum power of about 500 W, whereas that of the Pd-modified Ni foam cathodes reached 560 W. Moreover, both generated H_2 and O_2 gas products were high purity (H_2: 99.99% and O_2: 99.90%).

Finally, extended-time alkaline water electrolysis experiments were conducted on a single cell electrolyser setup with two different anodes. The cell's configurations comprised Ir-modified Ni foam cathode, whereas anodes were based on either electrooxidized, or else on Co-activated nickel foam electrode. Both electrode arrangements were characterized by similar cell's voltages to those previously reported for the Pd-activated Ni foam cathode/ electrooxidized Ni foam anode. Moreover, these new catalyst systems proved to be fairly durable and stable over the 24-hour galvanostatic tests.

Keywords: HER, OER, AWE, hydrogen, oxygen, Electrocatalysts, Ni foam, Cobalt, Molybdenum, Palladium, Electrolysis

2. Streszczenie

W niniejszej rozprawie doktorskiej zostały podjęte próby opracowania zaawansowanych elektrokatalitycznych materiałów na bazie pianki niklowej, które charakteryzowały się stosunkowo niską ceną produkcji oraz wysoką trwałością podczas długotrwałej pracy. Wysoce efektywne materiały elektrodowe w postaci katody oraz anody zostały wykorzystane odpowiednio w reakcjach wydzielania wodoru (Hydrogen Evolution Reaction; HER) oraz tlenu (Oxygen Evolution Reaction; OER). Poza wysoką stabilnością oraz efektywnością podczas długoterminowej pracy, materiały powinny charakteryzować się niską wartością nadpotencjału w stosunku do wyżej wymienionych reakcji. Proces rozkładu wody wymaga znacznego przekroczenia termodynamicznego napięcia o wartości 1.229 V. Dodatkowo materiały wykorzystane w pracy doktorskiej powinny charakteryzować się wysoką dostępnością w środowisku naturalnym, wysokim przewodnictwem elektrycznym oraz znacznie rozbudowaną elektrochemicznie czynną powierzchnią.

W związku z tym pierwsza część niniejszej rozprawy doktorskiej dotyczyła kompleksowych badań nad kinetyką katodowego procesu wydzielania wodoru. Proces ten badany był przy użyciu innowacyjnych, katalitycznych materiałów kompozytowych w postaci: niezmodyfikowanej pianki niklowej oraz pianki niklowej pokrytej niewielką ilością nanocząsteczek irydu. W celu osadzenia cząstek katalizatora na powierzchni materiału bazowego wykorzystano dwie metody depozycji, tj. spontaniczną oraz elektrochemiczną depozycję. Wszystkie badania elektrochemiczne przeprowadzono w trójkomorowej elektrochemicznej celi pomiarowej wykonanej ze szkła pyreksowego w roztworze 0,1 mol dm^{-3} NaOH, który był przygotowany z wykorzystaniem ultra-czystej wody (przy użyciu systemu Millipore Direct-Q3 UV; rezystywność wody wynosiła 18.2 MΩ cm).

Elektrochemiczne pomiary, tj. spektroskopia impedancyjna oraz kwazi-stacjonarne metody polaryzacyjne (krzywa Tafela) zostały przeprowadzone przy wykorzystaniu urządzenia

Solartron 12,608 W (Full Electrochemical System), składającego się z analizatora częstotliwości (FRA 1260) oraz elektrochemicznego interfejsu (EI 1287). Ponadto, została przeprowadzona analiza spektroskopowa badanych materiałów katalitycznych przy użyciu: skaningowej mikroskopii elektronowej (Scanning Electron Microscopy; SEM) oraz spektroskopii rentgenowskiej z dyspersją energii (Energy-Dispersive X-Ray Spectroscopy; EDX). W oparciu o wyznaczone parametry elektrochemiczne, tj.: rezystancję przeniesienia ładunku, gęstość prądu wymiany, pojemność, itp. zaobserwowano, że niewielkie ilości Ir osadzone na powierzchni uprzednio przygotowanego materiału bazowego w postaci pianki niklowej spowodowały znaczną poprawę ich aktywności katalitycznej w reakcji HER. Otrzymane podczas badań wyniki jasno ukazały pozytywny wpływ nanocząstek irydu na efektywność reakcji HER, co wskazuje na możliwość wykorzystania badanych kompozytowych materiałów katodowych w przemysłowych alkalicznych elektrolizerach wody.

Proces elektrochemicznego rozkładu wody zależy nie tylko od reakcji HER, ale również co ważniejsze od kinetyki reakcji OER. Podczas gdy katodowy proces wydzielania wodoru charakteryzuje się stosunkowo niską wartością nadpotencjału, proces OER uznawany jest za etap determinujący kinetykę i tempo całej reakcji elektrolizy wody. Drugą część niniejszej pracy doktorskiej poświęcono badaniom kinetyki procesu OER, które przeprowadzono na powierzchniowo zmodyfikowanej piance niklowej poprzez nałożenie niewielkich ilości platyny, katalizatorów w postaci metali z grupy przejściowej (kobalt i molibden) oraz na intensywnie elektroutlenionej piance niklowej. Zaskakująco, reakcja OER zachodziła znacznie sprawniej na piance niklowej zmodyfikowanej metalami nieszlachetnymi w porównaniu do pianki zmodyfikowanej Pt oraz elektroutlenionej *in situ,* które to materiały wykazały znacznie pogorszoną elektrochemiczną aktywność.

Trzecia część pracy dotyczyła wykonania praktycznych badań nad alkaliczną elektrolizą wody przy użyciu innowacyjnego systemu AWE w skali laboratoryjnej o mocy ok. 500 W, który zaopatrzony był w katody w postaci pianki niklowej zmodyfikowanej Pd lub niezmodyfikowanym materiałem bazowym, oraz w anody w postaci elektroutlenionej pianki niklowej. Zarówno katalityczna aktywność oraz stabilność proponowanych systemów AWE zostały zbadane metodami galwanostatycznymi oraz impedancyjnymi przy użyciu urządzenia Solartron 12,608 W Full Electrochemical System oraz zasilacza prądu stałego 30 V/30 A (PeakTech®). Dodatkowo, podczas pracy systemu AWE zostały pobrane próbki gazów O_2 oraz H_2, które powstały podczas procesu elektrolizy wody. W kolejnym etapie została sprawdzona ich czystość przy pomocy analizy chromatografii gazowej (GC), którą wykonano przy użyciu urządzenia Shimadzu GC2014, który dodatkowo był zaopatrzony w kolumnę chromatograficzną oraz detektor helowy z wyładowaniem impulsowym (PD-HID-Pulse Discharge Helium Ionization Detector). Na podstawie badań zaobserwowano, że system AWE składający się z katody w postaci niezmodyfikowanej pianki niklowej w połączeniu z anodą w formie elektroutlenionej pianki, uzyskał maksymalną moc o wartości 500 W, podczas gdy system składający się z katody w postaci pianki niklowej zmodyfikowanej Pd uzyskał maksymalną moc 560 W. Na podstawie analizy chromatograficznej oznaczono czystość gazów wyprodukowanych w procesie elektrolizy wody, która wyniosła 99,99% oraz 99,90% odpowiednio dla H_2 oraz O_2.

W ostatnim etapie pracy wykonano długotrwałe eksperymenty elektrolizy wody na pojedynczych celach, które składały się z dwóch układów anod, tj. elektroutlenionej pianki niklowej lub pianki zmodyfikowanej Co, oraz katody w postaci pianki zmodyfikowanej Ir. Oba badane układy uzyskały porównywalne wartości napięcia do uprzednio otrzymanych przez system składający się z katody w postaci pianki zaktywowanej Pd oraz anody w postaci elektroutlenionej pianki niklowej. Oba badane innowacyjne układy elektrodowe

charakteryzowały się wysoką trwałością oraz stabilnością podczas 24 godzinnych elektrochemicznych badań galwanostatycznych.

Słowa kluczowe: HER, OER, AWE, Elektrokatalizator, pianka niklowa, kobalt, molibden, pallad, elektrokataliza

3. Introduction

3.1. The importance of alkaline water electrolysis for the world's energy sector

Progressively growing global population and urbanization observed in the past decades have led to a radical increase in overall energy demand. The latter creates new economic and environmental challenges. In particular, one of the most important problems is how to ensure sufficient amount of electricity for all sectors of industry, public institutions, transportation and household facilities, and infrastructure. The above is strictly correlated to the global decarbonization demand [1-3]. Unfortunately, general world's energy sector is still predominantly based on non-renewable, traditional fossil fuels. The extraction and exceeding use of primary energy resources entail serious ecological and economic consequences, namely: severe environment degradation and gradual depletion of natural resources. The above results in rapidly rising level of atmospheric carbon dioxide (significant contribution to global climate change) and increasing electricity prices. Thus, establishing serious actions, aiming at solving climate problems, is of superior importance. In fact, consistent decarbonization of the global energy sector could be the quickest way to limit the emission of greenhouse gases (GHG) [3-4]. Thus, increasing share of renewable energy sources in the electricity sector plays a pivotal role in the near-to-zero carbon emission route. Incorporation of alternative and renewable energy sources (RES), such as: solar, wind, tidal and biomass to common use holds the key potential to mitigate climate changes [5-7]. Nevertheless, despite significant opportunities that renewable energy sources bring, there are also some challenges that hinder their full development. In fact, such important renewable energy devices as wind turbines or photovoltaic cells suffer from considerable time intermittency, with seasonal or even daily power output variations, as well as geographic limitations. Moreover, complex and confusing political regulations in many countries significantly limit their common use. Climate-dependance of the RES leads to the situations in which on some days the daily energy production is insufficient

to cover the demand, while during more favourable conditions the amount of generated electricity far exceeds its immediate use. Hence, the best solution for utilization of excess energy amount produced at peak hours could be incorporation of energy storage systems or heat magazines [8-11]. However, energy storage systems also suffer from some serious disadvantages. For example, batteries are characterized by limited energy conversion rates, their efficiency decreases over time and final disposal could potentially generate dangerous waste [12-13]. The ongoing efforts to develop clean and sustainable energy sources have accelerated with global need for electricity generation and its accumulation into different storage systems.

Recently, considerable attention by the energy market has been given to hydrogen. This energy carrier could be a promising solution to the fluctuations encountered by the renewable energy sources. In fact, coupling hydrogen with renewable energy sources may be the best way to decarbonize entire energy sector. A key idea in energy transformation is to utilize the surplus of electricity produced from the RES and to transform it into a chemical energy carrier in the form of hydrogen [14-16]. Then, hydrogen could conveniently be stored in highly pressurized, mobile tanks, or else it might be transported via hydrogen tailored gas pipelines.

Nowadays, hydrogen is predominantly generated via steam reforming of methane, coal gasification and hydrocarbon cracking processes, which not only require large amounts of input energy and expensive infrastructure, but also generate excess of carbon-based by-products. In connection with the decarbonization of the energy industry, renewable energy-powered alkaline water electrolysis (AWE) could be considered as an exceptional alternative, especially in the framework of power-to-gas concept [17-18]. It should also be stressed that with respect to the system's capital investment and durability, AWE technology is still considered superior to that of proton exchange membrane (PEM) design.

Moreover, the so-called *green hydrogen* (H produced via renewable energy sources) is considered the only, completely eco-friendly energy carrier with unlimited resources.

Combustion of hydrogen molecule in oxygen leads to the release of large amount of energy in the form of heat (Q), where water molecule is the only product of this reaction (see Eqn. 1 below). In addition, hydrogen is characterized by very high calorific value of energy density (*ca*. 120 MJ kg^{-1} or 33.6 kWh kg^{-1}), which is almost three times as high as that for diesel (45 MJ kg^{-1}) or gasoline (44 MJ kg^{-1}). Moreover, hydrogen is characterized by octane number of 130, as compared to 87 and 30 for basic gasoline and diesel fuel, respectively [19-27].

$$H_2 + \frac{1}{2}O_2 \rightarrow H_2O + Q \quad (1)$$

3.2.The mechanisms of HER and OER half-reaction

The process of water electrolysis consists of two simultaneously proceeding half-cell reactions, namely: cathodic hydrogen evolution reaction (HER) and anodic oxygen evolution reaction (OER). Hydrogen evolution proceeds at electrode potentials negative to the reversible H_2 potential. In alkaline environment, the HER mechanism at metal (M) electrode is based on a two-step reaction, involving water molecule and adsorbed hydrogen radical intermediate species (Eqns. 2 and 3 or 2 and 4) [28-34]:

$H_2O + e^- + M \rightarrow MH_{Ads} + OH^-$ (Volmer electrochemical discharge step) (2)

$H_2O + MH_{Ads} + e^- \rightarrow H_2 \uparrow + M + OH^-$ (Heyrovsky electrochemical desorption step) (3)

$2MH_{Ads} \rightarrow H_2 \uparrow + 2M$ (Tafel catalytic recombination step) (4)

On the other hand, the OER is a complex, four electron and four proton electrochemical process (Eqn. 5), which involves several intermediate steps (Eqns. 6 through 8). Initially, partial oxidation (deprotonation) of water molecule leads to the formation of surface-adsorbed OH_{Ads} species (Eqn. 6). Then, electron transfer and deprotonation of OH_{Ads} in the second step result in the formation of O_{Ads} (Eqn. 7), being a prerequisite for chemical recombination of O_{Ads} in the next step and generation of O_2 molecule in Eqn. 8 [35-39].

$$2H_2O \rightarrow 4H^+ + O_2 \uparrow + 4e^- \quad (5)$$

$$H_2O \rightarrow OH_{Ads} + H^+ + e^- \quad (6)$$

$$OH_{Ads} \rightarrow O_{Ads} + H^+ + e^- \quad (7)$$

$$2O_{Ads} \rightarrow O_2 \uparrow \quad (8)$$

In order to make water electrolysis a cost-effective process, the effectiveness of both half-reactions must be optimized. The above could conveniently be achieved through modification of the baseline electrode materials with highly active and simultaneously economical electrocatalyst materials [32-35, 37, 39].

4. Work Objectives

Major objectives of this work involved:

1. Preparation of innovative, highly catalytic and relatively inexpensive Ni foam-based electrode materials for cathodic generation of hydrogen (HER): **[Paper I]**,
2. Preparation of original, cost-effective Ni foam-based electrode materials for anodic generation of oxygen (OER): **[Papers II-III]**,
3. Construction of stack-innovative, laboratory-scale alkaline water electrolyser unit: **[Paper IV]**.

5. Materials and Methods

All details on the preparation of Ni foam-based electrodes, electrochemical cell, electrolyte solutions and experimental techniques employed for the purpose of this doctorate thesis were comprehensively described within the relevant publications that this thesis is based on **(Papers I** through **IV).** The purpose of this section is only to provide a reader with brief information and general principles that have been employed in this work.

5.1.Employed Techniques

Ac. Electrochemical Impedance Spectroscopy (EIS): it is a powerful, sensitive and non-invasive technique, which delivers important information (including resistance and capacitance parameters), leading to e.g. determination of the rates and mechanisms of various electrode processes, occurred at the electrode-electrolyte interface. The EIS measurements are commonly used to characterization of such electrochemical systems as: corrosion phenomena, batteries, supercapacitors and fuel cell devices. For a potentiostatic mode, the EIS measurement consists of applying a small sinusoidal voltage of a certain amplitude (<10 mV), which produces a current response in a sinusoidal form of the same frequency but shifted in phase. Examining the current response over a range of frequencies allows separation of electrode processes, which occur on different timescales [40-44].

Cyclic Voltammetry: it is a versatile electroanalytical technique employed to provide information about the reduction and oxidation (charge-transfer and mass-transport) processes occurring at the surface of working electrode. In this potentiodynamic technique, the potential of the working electrode (with respect to the reference one) increases linearly (triangular pattern is shown in schematic representation of Fig. 1 below) with time in a cyclic manner. Hence, during the measurement, the electrode potential (E, see Eqn. 9) is swept (at a sweep-rate, s: mV s^{-1} in time, t) back and forth between the lower and upper potential limits (where E_0 is an initial

electrode potential) and the current passing between the working and counter electrodes is recorded. Graphical relationship between the applied potential and recorded current is presented on the chart so-called "cyclic voltammogram" (CV) [45-46].

$$E = E_0 + s \times t \tag{9}$$

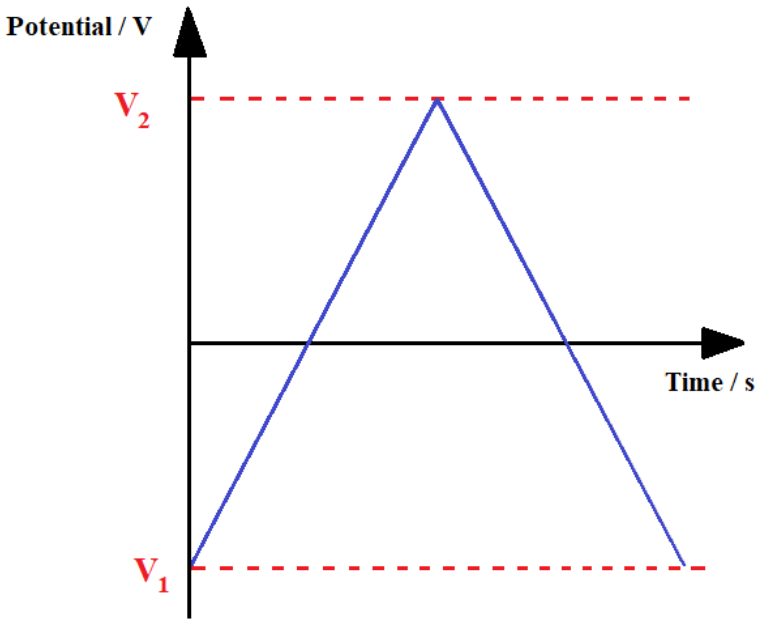


Figure 1 Triangular-shaped voltage sweep pattern in cyclic voltammetry technique.

Quasi Steady-State Tafel Polarization Plots: it is a commonly used technique for determination of the kinetics and other features of various electrochemical processes, e.g. reaction rates, exchange current-densities (j_0), overpotential (η), passivity and pitting susceptibility parameters, and cathodic/anodic Tafel slopes (b_c and b_a). The latter is considered a critical parameter for obtaining insightful information on the HER/OER mechanisms and effectiveness of electrode materials. Tafel tests are carried-out by recording current response to the electrode potential change at a low scan-rate, of e.g. 0.5 mV s^{-1}, whereas the Tafel plot is then presented as E vs. log I (or log j) [47-48].

Scanning Electron Microscopy (SEM): it is a versatile, non-invasive instrumental spectroscopy technique, which produces images of samples by scanning their surfaces with a focused beam of electrons. The electrons interact with atoms in the specimen, thus producing signals that contain information about the composition of the examined sample and its surface topography. Specimens could be examined by conventional SEM under high or low vacuum, or under environmental conditions [49-52].

Energy-Dispersive X-Ray Spectroscopy (EDX): it is a non-invasive analytical spectroscopy method (typically coupled with SEM) used for identifying and quantifying samples' elemental compositions. The atoms on the sample's surface are excited by the electron beam, thus emitting specific wavelengths of X-rays that are characteristic of the atomic structure of constituting elements. An energy dispersive detector is employed to analyze these X-ray emissions. Appropriate elements are allocated, yielding the composition of the atoms on the specimen's surface [53-55].

Gas Chromatography (GC): it belongs to a numerous group of chromatographic methods used both in science and industry. This separation technique is commonly used to detection of various components, residues or contaminants in a highly complex mixture, in this case in gaseous state. In principle, this method is used to separate components that are distributed between two phases, namely: stationary and mobile phases. The former is a liquid-based (stationary) medium whereas the latter utilizes an inert gas as a mobile phase. In GC, the separation phenomena are primarily based on differences of boiling points/vapor pressures and polarity variation of the components. The GC measurements start by introducing an examined sample *via* an injection port into injector. Then, gas carrier (mobile phase) passes through the inlet and sweeps the sample onto the column (stationary phase), at strictly determined temperature. Due to variation of chemical and physical properties of the components dissolved in the examined mixture, they travel through the chromatographic column with different

retention times. Then, they enter a detector, which provides an electronic signal being proportional to the amounts of eluting analytes [56-57].

5.2.Supporting Electrolytes, Base Catalytic Material and its Modifications

All supporting solutions were prepared by dissolving chemical reagents in ultra-pure water generated by Direct-Q3® Ultraviolet (UV) water purification system from Millipore or by Spring 30 s purification system from Hydrolab. Water processed through both systems was purified to reach a final resistivity of 18.2 MΩ cm at 25 ºC. For electrochemical examinations conducted for the purpose of this thesis, the following solutions were prepared:

- 0.1 M NaOH supporting solution from 99.996% sodium hydroxide pellets delivered by AESAR (Haverhill, MA, USA);
- 0.5 M H_2SO_4 supporting solution for periodic charging of auxiliary Pd/H_2 electrode was made from ultra-high purity stock sulphuric acid (SEASTAR Chemicals, BC, Canada) or 96% stock H_2SO_4 product from Merck (Darmstadt, Germany);
- 8 M KOH supporting solution was prepared from p.a. KOH pellets delivered by POCH (Gliwice, Poland).

Nickel foam (Ni foam): EQ-bcnf-16m, delivered by MTI Corporation (Richmond, CA, USA) was employed as a base electrode material to examine the kinetics of the HER and OER, as well as the efficiency of the electrolyser stack. The baseline catalytic material was high purity, 99.99% Ni material, having thickness of 1.6 mm, surface density of 346 g m^{-2} and porosity approaching 95%. Then, the following metal catalysts (and corresponding chemical reagents) were used for the modification of the base electrode material:

- Ir: iridium (III) chloride hydrate of 99.9% grade from Sigma Aldrich (St. Louis, MO, USA);

- Pt: chloroplatinic acid hexahydrate of 99.9% purity from Sigma Aldrich (St. Louis, MO, USA);
- Co: cobalt (II) chloride hexahydrate of 99.0% purity from Sigma Aldrich (St. Louis, MO, USA);
- Mo: ammonium heptamolybdate tetrahydrate (≥99.3% purity) delivered by Merck (Darmstadt, Germany);
- Pd: palladium (II) chloride (≥99.0% purity) provided by POCH (Gliwice, Poland).

Electrochemical modifications of the base Ni foam material were realized by means of catalyst (Ir, Co, Mo, Pt, Pd) electrodeposition (conducted in a galvanostatic mode at variable current-densities) or via spontaneous metal deposition through the employment of metal exchange processes under electrolytic conditions. On the other hand, an extensively electrooxidized Ni foam anode was prepared through extended cyclic voltammetry sweeps (100 cycles, carried-out over the potential range: 0.5-2.0 V vs. RHE, at a sweep-rate of 100 mV s^{-1}). Detailed information on the procedures for electrocatalysts preparation could be found within the monothematic list of articles (**Papers I** through **IV**).

6. Results and Discussion

The purpose of original scientific articles employed to form the basis of this Ph.D. thesis was to deliver innovative, electrocatalytically active and relatively cost-effective electrode materials, such as nickel foam (Ni foam) towards hydrogen and oxygen evolution reactions, with their potential application in a laboratory-scale alkaline water electrolyser system. Hence, the base material in the form of nickel foam was then modified through electrochemical/chemical deposition by very low amounts of nano-structured noble (Ir and comparatively: Pt, and Pd) or transition metals (Co, Mo), with the purpose of improving the electrochemical (HER and OER) activities of the baseline nickel foam material. Moreover, supplementary examinations were conducted to assess the durability of the employed electrode materials, in order to provide industrially applicable electrode composites.

6.1.Hydrogen Evolution Reaction

With constantly increasing importance of the RES, significant attention is given to the development of hydrogen technologies. Unfortunately, most of the commonly used H production methods are still based on fossil fuels, e.g. reforming of hydrocarbon sources, where methane is a worldwide key player. Although their widespread use and relatively inexpensive technology (per mass of generated H_2), these methods are burdened with large energy demand and excessive generation of CO_2, and heat as reaction by-products. Therefore, they are totally not in line with environmental zero emission line and regulations [14, 18].

On the other hand, electrochemical hydrogen evolution reaction is capable of producing ultra-pure hydrogen gas. Such-generated hydrogen, when coupled with alternative energy sources, e.g. solar or wind energy, could then be considered as an ideal (emission-free manufactured) green energy carrier [14]. For the HER performed under alkaline conditions, extremely desired are cathode materials that exhibit high corrosion resistance in alkaline media

and superior electrical conductivity. At the same time, they should be characterized by extensive, electrochemically active and catalytically modifiable surface area. The proposed in this work Ni foam baseline catalyst material possesses an exceptional HER performance in alkaline media. Furthermore, a highly porous nickel foam is characterized by large specific surface area, which is very important when fabricating the HER-active catalysts [58-62]. Usually, Ni foam is manufactured through chemical vapour deposition (CVD), electrochemical or electroless deposition technologies. In these methods, a molecular nickel is deposited on a polyurethane foam frame; then, the artificial material is etched or fired with the final formation of pure nickel foam porous structure [62]. For all alkaline water electrolysis tests, carried-out for the purpose of this thesis, electrochemically produced Ni foam was used as a baseline material to prepare both composite HER cathode and OER anode catalysts.

In this work, **Paper I** describes *a.c.* impedance characterization of the cathodic hydrogen generation, performed on Ni foam and Ir-modified Ni foam (*ca.* 0.1-0.3 wt. % Ir) electrodes immersed in 0.1 M NaOH as a supporting solution. Activation of the nickel foam samples with Ir electrocatalyst was performed by either a spontaneous or an electrochemical deposition method. The first approach was employed to produce two electrode samples, namely: SD1 and SD2 specimens, prepared by immersion of the base Ni foam material in $IrCl_3$ salt solution at 298 K for 30 and 300 s, respectively. Secondly, Ni foam/Ir composite electrodes were produced *via* electrodeposition of nanosized (*ca*. 10 nm) Ir particles onto Ni foam base material. Likewise, two electrodeposited Ni foam/Ir electrodes were prepared under the following experimental conditions: solution temperature was kept at 298 K, deposition current-densities were set at about 0.08 mA cm^{-2} for 600 s for ED1 and 5.25 mA cm^{-2} for 1200 s for ED2 electrode.

The recorded EIS results presented in **Paper I** clearly indicated that deposition of small amounts of nanosized particles of iridium *via* spontaneous and electrochemical deposition

methods, significantly improved the electrocatalytic activity of the baseline material towards the HER. The Nyquist impedance plots recorded for all the examined samples exhibited single, partial and somewhat depressed semicircles that were strictly related to a single-step Faradaic process of the HER charge transfer, at all examined potentials in the investigated frequency range. Hence, the improvement of the electrode kinetics towards the HER was revealed in a radical reduction of the charge-transfer resistance, R_{ct} parameter (see detailed results in Table 1 below). Thus, at the overpotential of 100 mV, both SD1 and SD2 samples exhibited significantly reduced (by *ca*. 3-5 times) values of the Faradaic reaction resistance (219 and 269 Ω cm^2 respectively), as compared to those of unmodified and chemically etched Ni foam samples (1220 and 923 Ω cm^2, correspondingly). Similarly, modification of the Ni foam by surface deposition of Ir nanoparticles *via* dc. driven method led to a substantial reduction of the R_{ct} parameter, namely by *ca.* 10× for both the ED1 (102 Ω cm^2) and ED2 (87 Ω cm^2) samples, at the corresponding overpotential of 100 mV. In general, deposition of the iridium catalyst's nanoparticles provides an overall decrease of the R_{ct} parameter values over the whole range of examined overpotentials (from -100 to -400 mV) for all tested HER catalyst samples. Table 1 and Figs. 2a, and 2b below present detailed characteristics of the *ac.* impedance behaviour and representative complex-plane impedance plots of the HER, studied at the Ir-modified Ni foam electrodes in 0.1 M NaOH supporting solution, respectively. Moreover, a pre-treatment of the Ni foam electrode samples with hot hydrochloric acid led to a significant growth of the double-layer capacitance, C_{dl} parameter, as compared to that for *as received* Ni foam electrode. The above reflects considerably expanded electrochemically active surface area, which is strictly associated with the removal of the passive oxide layer from the Ni foam surface, in addition to the surface etching effect [60-62]. Consequently, the pre-treated electrode samples showed significant increase of the C_{dl} (capacitance variable T) parameter for the corresponding overpotential values. For example, at η= 100 mV the C_{dl} values increased by *ca*. 5.9 times

(120.7 μF cm^{-2} $s^{\varphi-1}$), 3.8× (77.5 μF cm^{-2} $s^{\varphi-1}$) and 10.8× (220.4 μF cm^{-2} $s^{\varphi-1}$) for the etched Ni foam, SD1 and ED2 samples, respectively, as compared to the unmodified Ni foam electrode (20.4 μF cm^{-2} $s^{\varphi-1}$). It is clearly visible that upon overpotential augmentation (from -100 to -400 mV/RHE), significant reduction of the double-layer capacitance parameter is observed (see Table 1). It is a result of partial blocking of electrochemically available surface area by freshly generated hydrogen bubbles, which accelerates along with increased cathodic overpotentials.

Table 1 Electrochemical parameters (with their standard deviations) obtained for HER, recorded on Ni foam (*as received* and etched) and Ir-modified (spontaneously deposited: SD 1 and SD 2, and electrodeposited: ED 1 and ED 2) Ni foam electrodes in contact with 0.1 M NaOH.

***E*/mV**	**R_{ct}/Ω cm^2**	**C_{dl}/μF cm^{-2} $s^{\varphi-1}$**	**R_{ct}/Ω cm^2**	**C_{dl}/μF cm^{-2} $s^{\varphi-1}$**
	***As received* Ni foam**		**Etched Ni foam**	
-100	1220 ± 3	20.4 ± 0.2	923 ± 8	120.7 ± 2.3
-150	509 ± 2	19.2 ± 0.3	819 ± 5	90.4 ± 1.2
-200	273 ± 13	17.8 ± 0.4	400 ± 2	68.7 ± 1.0
-250	156 ± 10	15.9 ± 0.8	179 ± 1	52.6 ± 1.1
-300	106 ± 1	15.3 ± 0.9	90 ± 1	47.0 ± 1.6
-350	79 ± 1	17.4 ± 1.3	58 ± 1	47.8 ± 1.8
-400	60 ± 1	13.2 ± 0.9	42 ± 1	46.5 ± 2.0
	Ir-activated Ni foam: SD 1		**Ir-activated Ni foam: SD 2**	
-100	219 ± 2	77.5 ± 2.7	269 ± 1	75.7 ± 0.9
-150	215 ± 2	56.0 ± 1.5	192 ± 2	70.1 ± 1.3
-200	150 ± 1	53.8 ± 1.6	133 ± 1	63.0 ± 1.3
-250	99 ± 1	52.2 ± 3.1	93 ± 2	53.0 ± 2.6
-300	66 ± 1	59.5 ± 4.3	66 ± 1	49.4 ± 1.8
-350	48 ± 1	49.4 ± 3.3	48 ± 1	48.8 ± 2.1
-400	37 ± 1	45.0 ± 2.1	37 ± 1	45.5 ± 1.8
	Ir-activated Ni foam: ED 1		**Ir-activated Ni foam: ED 2**	
-100	102 ± 1	168.5 ± 3.7	87 ± 1	220.4 ± 4.2
-150	88 ± 1	142.4 ± 4.3	79 ± 1	144.3 ± 3.9

-200	76 ± 1	132.2 ± 4.3	70 ± 1	135.2 ± 4.0
-250	61 ± 1	114.9 ± 3.5	61 ± 1	129.6 ± 5.0
-300	52 ± 1	108.1 ± 4.0	52 ± 1	123.3 ± 4.7
-350	44 ± 1	99.4 ± 6.6	44 ± 1	104.3 ± 3.1
-400	47 ± 1	93.6 ± 3.4	36 ± 1	95.2 ± 4.1
j_0 (*as received* Ni foam) = 5.9×10^{-6} A cm^{-2} j_0 (etched Ni foam) = 3.9×10^{-6} A cm^{-2} j_0 (SD1) = 1.3×10^{-5} A cm^{-2} j_0 (ED1) = 4.6×10^{-5} A cm^{-2} j_0 (ED2) = 5.6×10^{-5} A cm^{-2}				

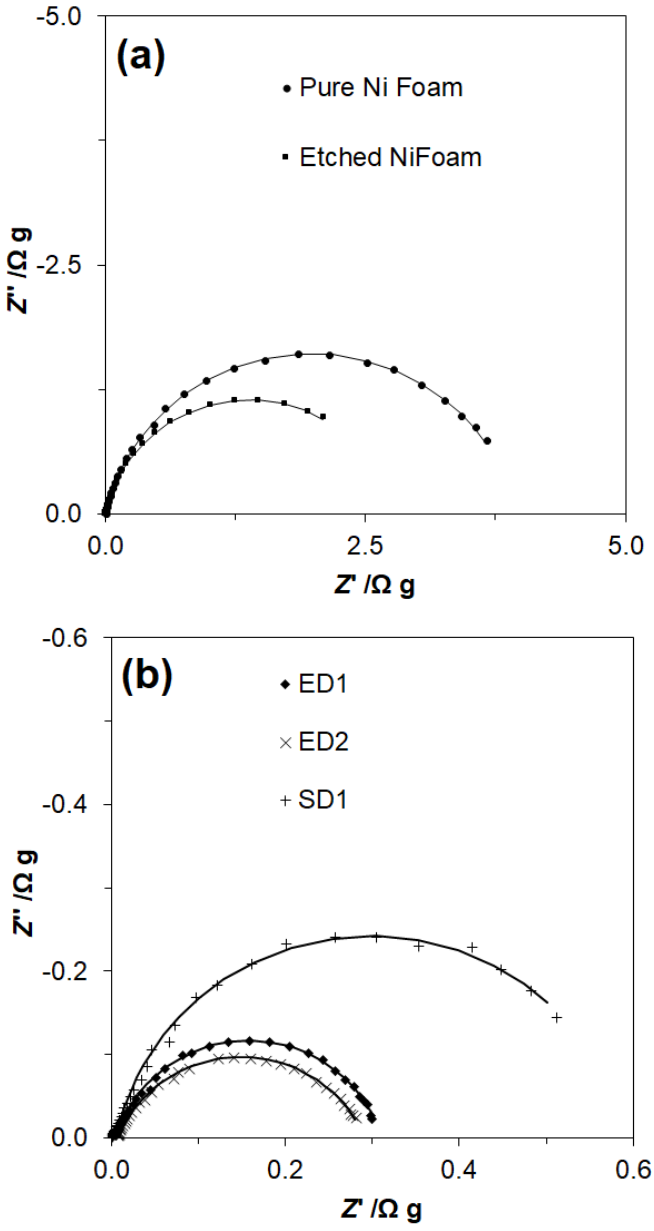


Figure 2 Complex-plane impedance plots for HER, carried out on fresh (*as received*) and etched Ni foam electrode surfaces **(a)** in contact with 0.1 M NaOH, recorded at 298 K for the potential of −100 mV (vs. RHE); **(b)** As above, but recorded on Ir-activated Ni foam electrodes via electrodeposition of iridium (ED 1 and ED 2 samples) and spontaneous deposition of Ir (SD 1 electrode).

Similar electrochemical HER studies, which covered the employment of Ni foam base material modified with noble and other types of electrocatalysts, were undertaken in other works from this laboratory [63, 64] and by other authors [65, 66]. Hence, Table 2 below presents values of the charge-transfer resistance and double-layer capacitance parameters recorded on the Ir-modified Ni foam electrodes in this work, and comparatively those obtained on analogous catalyst materials, reported earlier by Pierozynski et al. [63], Pierozynski and Mikolajczyk [64], Liu et al. [65] and Gao et al. [66].

Thus, the R_{ct} and C_{dl} parameters obtained for the Ir-modified Ni foam catalysts in this work fairly well compare (or in some cases even outperform) with different catalyst-modified Ni foam composites, already reported in available literature. Here, the ED2 sample was chosen as it provided the best catalytic activity among the examined Ir-activated Ni foam electrodes. This sample exhibited significantly lower values of the R_{ct} parameter than the palladium-activated electrode (~0.1 wt.% Pd), upon the corresponding overpotential magnitude [63]. Furthermore, the catalytic HER activity of the ED2 sample is comparable to that of Ni foam activated with ruthenium (~0.1 wt.% Ru) [63]. However, it should also be noted that in-situ facilitation of substrate activation process led to a significant HER activity enhancement of Pt-supported Ni foam composite electrode [64] (Table 2).

Furthermore, recent works by Liu et al. [65] and by Gao et al. [66] provided interesting HER results produced on analogous materials, namely: $NiCo_2S_4/Ni_3S_2$- and Ni-Se-Cu-modified Ni foam composites. Nevertheless, unclear determination and employment of electrochemically active surface area to carry-out calculations by the authors of these articles unable to make any

reasonable comparisons to the results obtained on the iridium-activated nickel foam by the author of this thesis (see Table 2 below and Refs. 65, and 66 for details).

Table 2 Comparison of the electrochemical parameters for HER derived from electrochemical impedance spectroscopy technique at the surfaces of Ni foam baseline surface, modified with different catalyst materials, examined under alkaline conditions.

Catalyst material	**Electrolyte**	R_{ct}/Ω cm^2	C_{dl}/μF cm^{-2} s$^{φ-1}$	η/mV	**Refs.**
Ir-modified Ni foam	0.1 M NaOH	87 (0.285 Ω g/5.83 Ω)	220.4 (66,873 μF g^{-1})	100	This work
		70 (0.229 Ω g /4.682 Ω)	135.2	200	
Pd-modified Ni foam	0.1 M NaOH	0.67 Ω g	117,414 μF g^{-1}	100	[63]
Ru-modified Ni foam	0.1 M NaOH	0.25 Ω g	83,042 μF g^{-1}	100	[63]
Pt-modified Ni foam	0.1 M NaOH	0.056 Ω g	682,063 μF g^{-1}	100	[64]
$NiCo_2S_4$/Ni_3S_2 -modified Ni foam	1.0 M KOH	2 Ω	113,500 μF cm^{-2}	200	[65]
Ni-Se-Cu-modified Ni foam	1.0 M KOH	11.05 Ω	25,800 μF cm^{-2}	200	[66]

Moreover, the exchange-current density (j_0) and Tafel slope (b_c) parameters were derived for the Ir-activated Ni foam electrodes from potentiostatic Tafel polarization plots illustrated in Fig. 3. Thus, the j_0 parameter for the examined electrodes reached the following values: 1.5×10^{-5}, 4.1×10^{-5} and 3.7×10^{-6} A cm^{-2} for the SD1, ED1 and chemically etched Ni foam samples, respectively. It is important to note that all Tafel-recorded j_0 values were very close to those *ac*. impedance-derived exchange current-densities (see bottom of Table 1). Then, the recorded cathodic Tafel slopes (b_c) approached 154, 98 and 77 mV dec^{-1} for the etched, ED1 and SD1 Ni foam samples, correspondingly. The lowest value of b_c recorded for the SD1 electrode suggests the highest electrocatalytic effectiveness for the HER amongst the examined Ni foam-based cathodes. These results suggest that the HER most likely undertakes the Volmer-Heyrovsky pathway on the examined Ni foam composite electrodes [34].

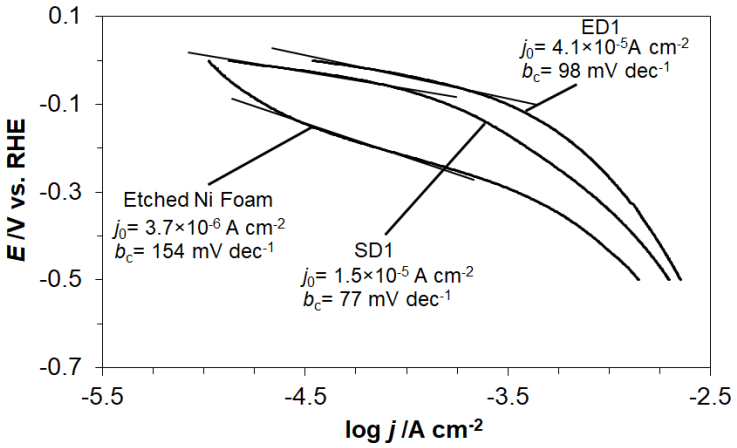


Figure 3 Quasi-steady-state potentiostatic cathodic Tafel polarization curves (recorded at a scan-rate of 0.5 mV s^{-1}) for etched Ni foam, ED1 and SD1 electrodes, carried out in 0.1 M NaOH solution.

It has to be stated that the recorded j_0 and b_c parameters for the Ir-modified Ni foam electrode samples are generally comparable to those previously recorded in this laboratory on other nickel foam-based electrocatalysts, produced via Pd, Ru and Pt nanoparticle modifications [63, 64]. Interestingly, other Ni foam-based HER composite catalysts (Ni-Cu dendrite, Ni-Mo-P film and Ni-P nanorods deposits) exhibited analogous HER behaviour (most likely a prevailing effect of radical expansion of electrochemically active surface area) in alkaline media to that reported here for the iridium-modified nickel foam materials (see Refs. 67-69 and Table 3 below).

Table 3 Comparison of the electrochemical parameters for HER, obtained through Tafel polarization plots at the surfaces of different catalyst materials, under alkaline conditions.

Electrode material	**Electrolyte**	**j_0/ A cm^{-2}**	**b_c/ mV dec^{-1}**	**Reference**
ED1	0.1 M NaOH	4.1×10^{-5}	98	This work
Ni-Cu dendrite-modified Ni foam	1.0 M KOH	-	82	[67]
Pd-modified Ni foam	0.1 M NaOH	1.1×10^{-5}	65	[63]
Ru-modified Ni foam	0.1 M NaOH	1.4×10^{-5}	84	[63]
Pt-modified Ni foam	0.1 M NaOH	2.0×10^{-5}	73	[64]
Ni-Mo-P film on Ni foam	1.0 M KOH	-	87	[68]
Ni-P nanorods on Ni foam	1.0 M KOH	2.04×10^{-5}	75	[69]

6.2.Oxygen Evolution Reaction

In contrast to the HER, the anodic-half-cell reaction of water decomposition, namely Oxygen Evolution Reaction (OER) is more demanding and involves four sequential electron-coupled charge transfer steps. Consequently, additional energy is required for the formation of the O=O bond, and the anodic oxygen generation in the-state-of-the-art is defined as a rate-determining step for the process of alkaline water electrolysis [37, 39]. With respect to facilitation of the OER, this doctoral dissertation thesis covers two published scientific articles (**Papers II** and **III**) on innovative anode materials towards improving the kinetics of electrochemical generation of oxygen. Similarly to the HER, the most desirable electrode and catalyst materials should possess the following features: high electrical conductivity, extended mechanical durability, exceptional anti-corrosive properties in concentrated alkaline media and respectively minimized reaction overpotentials. Such catalyst materials should also be relatively unexpensive, thus enabling their practical, commercial applications.

Hence, **Paper II** covers examination of the efficiency of oxygen evolution reaction in 0.1 M NaOH solution on: *as received* Ni foam, surface electrooxidized and Pt-activated (~0.20 wt.%, prepared via spontaneous platinum deposition) nickel foam materials. On the other hand, examination of Ni foam-based transition metal OER catalysts, namely: Co- (~1 wt.%) and Mo- (~0.28 wt.%) is described in **Paper III**. Here, modification of the base nickel foam material with Co- and Mo- nanoparticles was carried-out by electrochemical deposition methods performed at 298 K, at current-densities of *ca*. 0.5 and 5.0 mA cm^{-2}, respectively. The kinetics of oxygen formation were evaluated in 0.1 M NaOH supporting solution through the application of *ac.* impedance spectroscopy, cyclic voltammetry and Tafel polarization techniques.

Electrochemically made Ni foam material was found to exhibit superior catalytic properties towards oxygen evolution reaction in 0.1 M NaOH solution (**Paper II**). The latter is a combined effect of its highly-porous catalyst structure, as well as a natural tendency for nickel

to develop intrinsic surface oxide layers. However, extended surface electrooxidation treatment (carried-out by cyclic voltammetry: 100 CV sweeps carried-out at a sweep-rate of 100 mV s^{-1}, over the potential range 0.5-2.0 V), as well as Pt-activation of fresh nickel foam electrode, both resulted in significant deterioration of initial OER catalytic activity of the baseline foam material (see Fig. 4a).

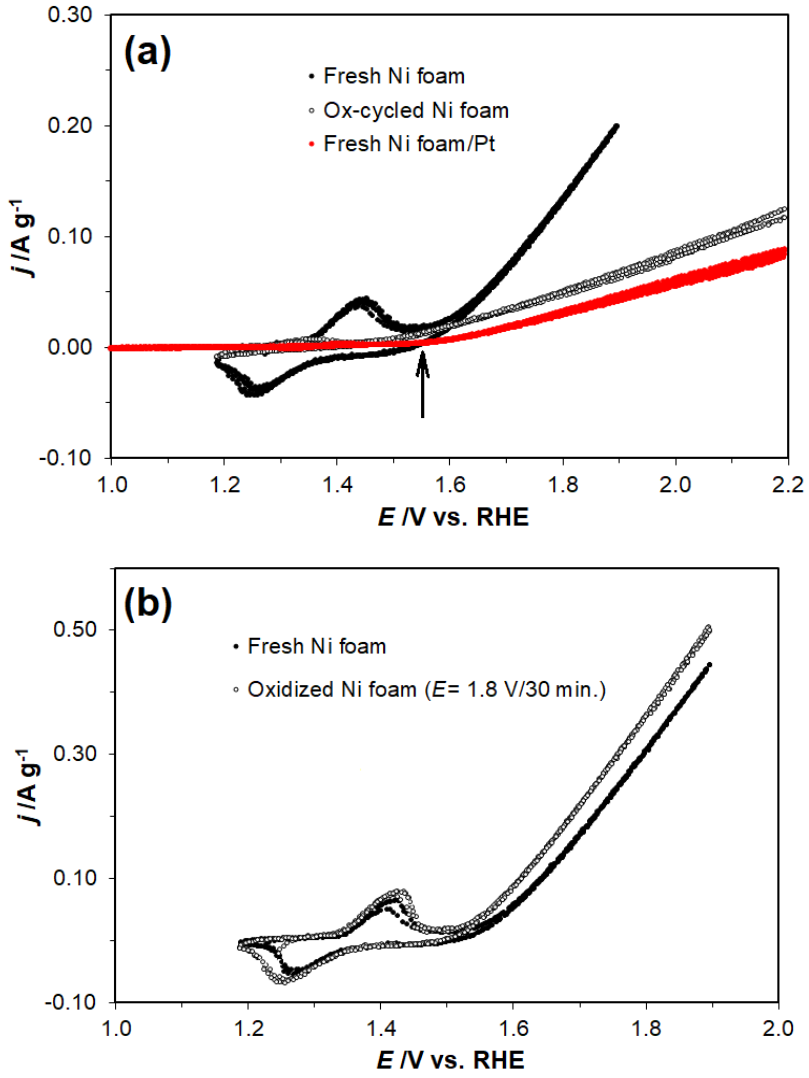


Figure 4 (a) Cyclic voltammograms recorded for pure, electrochemically oxidized and Pt-modified Ni foam electrodes in contact with 0.1 M NaOH (at 20 ^{o}C), carried-out at a sweep-rate of 50 mV s^{-1}; (**b)** As in (a) above, but recorded for pure and electrochemically oxidized (carried-out by potential hold at 1.8 V/RHE for 30 minutes) Ni foam electrodes.

The former is most likely related to a gradual formation of poorly conductive nickel oxide layer [excessive formation of Ni (IV) film] and the latter results from the fact that Pt itself is much less catalytic towards the OER than nickel-based materials. However, it has to be stated that under moderate oxidation conditions (i.e. for a potential hold procedure, carried-out at 1.8 V over the period of 30 minutes), the Ni foam electrode exhibited significant enhancement of the OER activity, which could clearly be seen in Fig. 4b above. Nevertheless, the cyclic voltammetry-deactivated Ni foam electrode could then become partly rejuvenated by means of galvanostatic, electrochemical reduction treatment (see Fig. 2d in **Paper II**). The idea behind this procedure is to prevent from excessive formation of Ni (IV), at the expense of Ni (III) species. In general, the latter complies with an anode rejuvenation practice described by Mellsop et al. (Ref. 31 in **Paper II**).

Furthermore, *ac*. impedance spectroscopy method proved to be an ideal tool for the examination and periodical monitoring of the oxygen evolution kinetics. For the electrode potentials positive or equal to 1.5 V vs. RHE, all impedance-examined Ni foam-based electrodes exhibited two, "depressed" semicircles, in the explored frequency range (see examples of Nyquist/Bode impedance plots in Figs. 4b through 4d of **Paper II**). Here, a circuit model containing two CPE-*R* elements (two time constants, see Fig. 4f in **Paper II**) was employed to characterize the recorded impedance behaviour, where the high-frequency (CPE/C_{dl}-R_{ct}) arc corresponds to the kinetics of the oxygen evolution reaction (interfacial charge-transfer reaction step), whereas the intermediate/low-frequency semicircle (CPE/C_{Ads}-R_{Ads}) is related to the surface adsorption of the reaction intermediates [i.e. $NiO(OH)_2$ species, see **Paper II** for details]. The CPE element was used in the circuit in order to account for the capacitance dispersion effect, represented by distorted semicircles in the Nyquist impedance plots [70]. Also, no diffusion type impedance behaviour was observed within the impedance diagrams down to the frequency of 50 mHz.

Hence, for the fresh Ni foam electrode the recorded R_{ct} parameter decreased from 1.11 Ω g at 1.5 V/RHE (reaction overpotential η = 270 mV) to 0.01 Ω g at the potential of 1.9 V (η = 670 mV). Simultaneously, the double-layer capacitance, C_{dl} parameter diminished from 23,540 to 520 μF g^{-1} $s^{\varphi 1-1}$ for the same potential range. The latter effect most likely results from substantial blocking of the electrochemically active electrode surface by freshly formed O_2 bubbles, which could easily be envisaged for a complex and porous Ni foam electrode structure, especially at increased anodic overpotentials. Thus, as expected the oxygen evolution process becomes significantly facilitated upon augmentation of the dc. electrode potential. However, the reported in Table 4 R_{Ads} parameter values are fundamentally greater than those recorded for the R_{ct}. This implies that the OER process is governed by the adsorption kinetics of the reaction intermediates. It should be acknowledged here that the impedance results obtained in this work are generally in-line with those OER impedance studies presented by Costa et al. and by Franco et al. on β-PbO_2 electrodes, by Doyle and Lyons on multi-cycled iron oxy-hydroxide films and by Lyons, and Brandon on passive oxide-covered polycrystalline Ni electrodes (see correspondingly Refs. 36, 37, 1 and 2 in **Paper II**).

Furthermore, extended surface electrooxidation (100 CV cycles carried-out at a sweep-rate of 100 mV s^{-1} over the potential range 0.5-2.0 V/RHE) resulted in significant OER deactivation of the nickel foam electrode. Hence, for the potential of 1.5 V, "deactivated" R_{ct} rose to 1.23 Ω g from an initial value of 0.71 Ω g (the potentials labelled as "1.5 ox." and "1.5 in." in Table 4). Simultaneously, the deactivated Ni foam electrode is characterized by radically reduced values of double-layer capacitance parameter, which implies that expanded Ni foam surface oxidation leads to a gradual development of thick and rather poorly conductive nickel oxide layer. Then, for surface electrooxidized Ni foam performed *via* the 1.8 V/RHE potential hold, the recorded R_{ct} values were considerably smaller (facilitation of the OER process) than

those obtained prior to the oxidation treatment, whereas the C_{dl} parameter exhibited only about 50 % reduction (compared with *ca*. 95 % C_{dl} decrease in the former case).

Finally, platinum-activated nickel foam electrode catalyst is characterized by significantly inferior OER kinetic characteristics to those for the pure Ni foam material. The latter is primarily evidenced through increased values of the R_{ct} and R_{Ads} parameters (along with nearly steady C_{dl} behaviour) over the entire examined overpotential range (Table 4). In fact, as argued by van Drunen et al. in Ref. 71, Pt nanoparticles present on the surface of Ni foam could "physically block regions of the underlying Ni, thus reducing the effective electrode's surface area". The above is in good agreement with the fact that unlike for hydrogen evolution phenomenon, for the oxygen evolution reaction platinum (including Pt nanodeposits) exhibits considerably inferior catalytic properties to those of nickel and Ni-based materials [71].

Table 4 Electrochemical resistance and capacitance parameters for OER, obtained on fresh, electrooxidized and Pt-activated Ni foam electrodes in contact with 0.1 M NaOH, at 20 ^{o}C (reproducibility about 10-15 %, $\chi^2 = 7\times10^{-5}$ to 4×10^{-4} and 1×10^{-3} for the potential of 1.9 V).

***E*/ V**	**R_{ct}/ Ω g**	**C_{dl}/ µF g^{-1} s$^{\varphi 1-1}$**	**R_{Ads}/ Ω g**	**C_{Ads}/ µF g^{-1} s$^{\varphi 2-1}$**
Pure Ni foam				
1.5	1.11 ± 0.11	23,540 ± 1,765	13.13 ± 0.55	8,980 ± 651
1.6	0.30 ± 0.03	55,055 ± 6,175	0.98 ± 0.06	59,140 ± 6,032
1.7	0.09 ± 0.01	11,982 ± 1,074	0.27 ± 0.02	112,678 ± 7,775
1.8	0.04 ± 0.00	2,385 ± 155	0.17 ± 0.01	117,412 ± 7,514
1.9	0.01 ± 0.00	520 ± 35	0.15 ± 0.01	93,895 ± 5,394
Electrooxidized (Ox-cycled) Ni foam				
1.5 in.	0.71 ± 0.07	63,250 ± 6,546	1.31 ± 0.04	68,478 ± 4,379
1.5 ox.	1.23 ± 0.13	3,226 ± 347	6.40 ± 0.24	6,286 ± 685
Electrooxidized (*E*= 1.8 V/30 min.) Ni foam				
1.5 in.	0.96 ± 0.08	116,540 ± 2,715	10.34 ± 0.07	20,158 ± 3,003
1.5 ox.	0.10 ± 0.01	56,162 ± 6,178	3.41 ± 0.14	101,240 ± 11,642

Pt-modified Ni foam				
1.5	1.98 ± 0.15	5,676 ± 496	15.98 ± 0.37	4,336 ± 412
1.6	1.50 ± 0.11	4,040 ± 373	6.90 ± 0.35	3,158 ± 316
1.7	0.41 ± 0.04	8,336 ± 500	2.27 ± 0.16	20,612 ± 1,288
1.8	0.10 ± 0.01	5,677 ± 125	2.34 ± 0.13	35,240 ± 2,824
1.9	0.06 ± 0.00	550 ± 40	1.35 ± 0.03	10,374 ± 633

Moreover, Fig. 5 below presents –log R_{ct} vs. T^{-1} Arrhenius-type plot, constructed based on the R_{ct}= f(T) impedance results. Such-estimated, experimental electrochemical activation energy, E_A for the potential just positive to the OER's onset potential approached 31.6 and 54.5 kJ mol^{-1} for the unmodified and the Pt-activated nickel foam electrodes, respectively. These results correspond fairly-well to those E_A values reported for NiFe oxide, IrO_2-Ta_2O_5 and Ti/Pt/SnO_2-Sb anode materials (see Refs. 40-42 in **Paper II**).

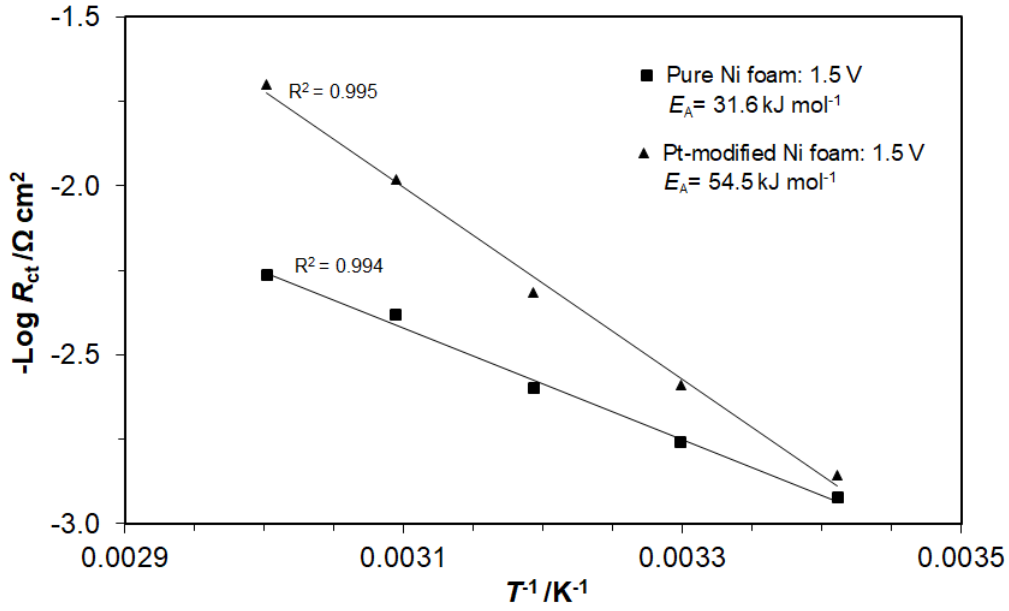


Figure 5 Linear plots of –log R_{ct} vs. T^{-1} for OER on pure and Pt-activated Ni foam electrode surfaces in 0.1 M NaOH solution, carried-out at the potential of 1.5 V.

On the other hand, cyclic voltammetry (CV) characterization of the surface oxidation process on fresh, Co- and Mo-modified Ni foam electrodes in 0.1 M NaOH solution during 50 CV sweeps, carried-out over the potential span 1.2–1.9 V/RHE with a scan rate of 50 mV s^{-1} (only three last sweeps are presented) is illustrated in Fig. 6 below (**Paper III**). Thus, for pure and Co-modified nickel foam samples, the CV profiles displayed an oxidation peak (centred at ca. 1.49 and 1.45 V, correspondingly) along with a cathodic reduction peak (starting around 1.3 V). The Mo modification caused a shift of the oxidation peak to more positive potentials than that for pure Ni foam. In contrast, the reduction peak was no longer visible, as it was most likely moved outside the measured potential range. These features refer to the electrochemical formation of the surface β-NiOOH phase and its later reduction to β-$Ni(OH)_2$ layer, respectively (Eqn. 10).

$$\beta - \mathrm{Ni(OH)_2} + OH^- \leftrightarrow \beta - \mathrm{NiOOH} + H_2O + e^- \quad (10)$$

It should be noticed however in Fig. 6 that for both the Co and Mo-activated Ni foam electrodes, the recorded current-densities were significantly higher than those derived for the unmodified nickel foam anode.

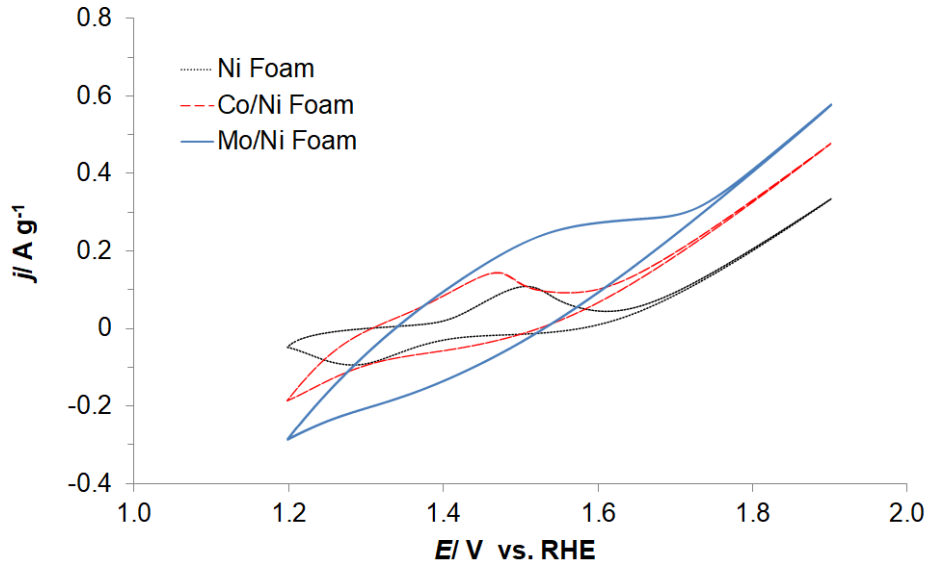


Figure 6 Cyclic voltammogram curves of oxidized, pure Ni, Co- and Mo-activated Ni foam electrodes, in contact with 0.1 M NaOH medium (at 20 °C), carried-out at a scan-rate of 50 mV s^{-1} for the potential span 1.2–1.9 V.

Furthermore, Tafel polarization plots were recorded over low overpotential range at room temperature for electrochemically oxidized pure Ni foam, Mo- and Co-modified Ni foam electrodes (see Fig. 3 in **Paper III**). Hence, the Tafel-derived exchange current-densities, j_0 values for the OER came to 7.1×10^{-11}, 7.0×10^{-8} and 9.6×10^{-8} A cm^{-2}, correspondingly, for the electrochemically oxidized Ni foam, Co- and Mo-modified nickel foam composites. Pre-electrooxidation of Ni foam surfaces proved to be necessary in order to increase an initial value of the j_0 parameter by 3.7 times, in contrast to an analogous, but unmodified nickel foam-based electrode (**Paper II**, also compare with the j_0= 5.5×10^{-8} A cm^{-2} recorded for the platinum-activated nickel foam there).

In addition, the OER exchange current-densities were also derived for high overpotential range (η = 270–620 mV with 50 mV potential increments) based on the linear dependence of -log R_{ct} vs. overpotential (see Refs. 43-44 in **Paper II**). Hence, the impedance-based j_0 values for the studied overpotential range came to about 6.1×10^{-5} A cm^{-2} for the *as received* Ni foam sample. However, significantly higher exchange current-densities were

recorded for both Co- and the Mo-modified Ni foam samples, i.e., 2.9×10^{-4} and 1.0×10^{-4} A cm^{-2}, correspondingly (see Figure 6 in **Paper III**).

Finally, the electrochemical impedance spectroscopy was applied, in order to further characterize the electrocatalytic properties of Co/Mo-activated nickel foam electrodes towards the OER. Analogously to the impedance results presented in **Paper II**, all Ni foam-based electrodes exhibited two depressed semicircles, where the high-frequency arc could be associated with the kinetics of the oxygen evolution reaction (interfacial charge-transfer reaction step). In contrast, the intermediate/low-frequency semicircle corresponds to the surface adsorption of the reaction intermediates (see Nyquist impedance plots in Fig. 7 below). The electrochemical parameters (Faradic reaction resistance: R_{ct}, adsorption resistance for reaction intermediates: R_{Ads}, double-layer capacitance: C_{dl} and pseudo-capacitance: C_{Ads}) were obtained by means of two constant phase element (CPE)-modified Randles equivalent circuit model (Figure 5 in **Paper III**), and their values are presented in Table 2 there. Again, the CPE element was used within the circuit to account for the capacitance dispersion effect.

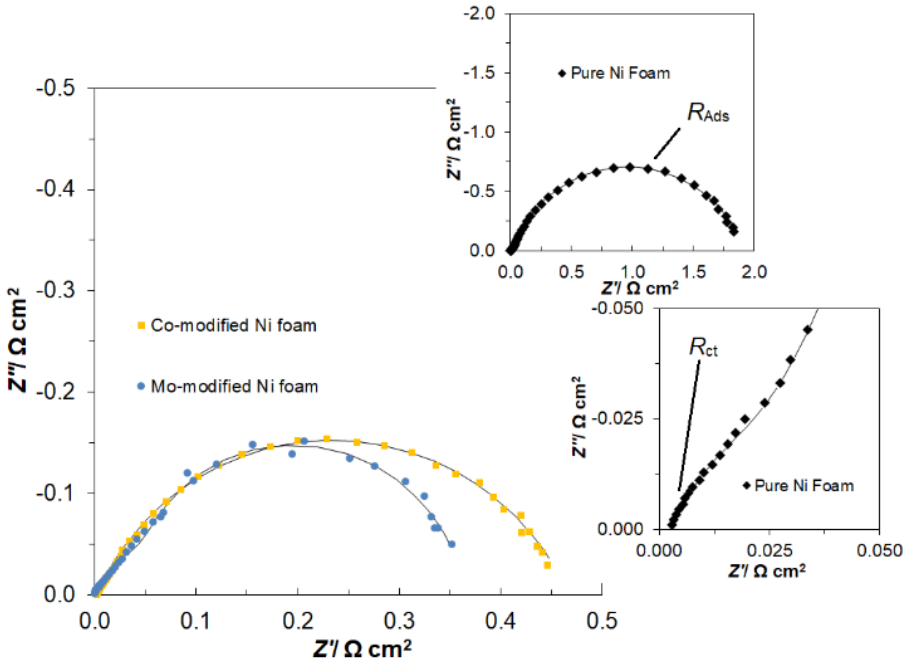


Figure 7 Electrochemical impedance Nyquist plots for OER on oxidized Ni foam, Co- and Mo-modified Ni foam electrode surfaces in contact with 0.1 M NaOH, at 20 °C for the potential of 1.6 V vs. RHE.

Thus, for the oxidized Ni foam electrode, the recorded R_{ct} parameter diminished from 0.187 Ω g (at η = 270 mV) to 0.047 Ω g at η = 620 mV, respectively. Similarly, the C_{dl} parameter decreased from the value of 120,933 to reach 8720 μF g^{-1} $s^{\varphi 1-1}$ for the same overpotential span (see Table 2 of **Paper III** for details). The above effect could again be associated with substantial blocking of the electrode surface by freshly formed O_2 bubbles, which could easily be visually noticed, especially at increased anodic overpotentials. Simultaneously, the value of the R_{Ads} parameter reduced from 41.756 to 0.123 Ω g for the corresponding overpotential range, while the C_{Ads} parameter oscillated between an initial value of 144,293 (at η=270 mV) and a minimum value of 67,867 μF g^{-1} $s^{\varphi 2-1}$, recorded at 420 mV. The latter understandably implies that the kinetics of the OER become facilitated upon the rise of the dc. electrode potential. However, as the R_{Ads} values are essentially larger than those recorded for the R_{ct} parameter, the OER process is most likely limited by the reaction intermediates´ adsorption kinetics (Refs. 23,34 in **Paper III**).

Then, the recorded values of the R_{ct} parameter for the Co- and Mo-modified Ni foam electrodes were radically reduced (as compared to the catalyst-unmodified Ni foam) and ranged from 0.052 to 0.022 Ω g and from 0.081 to 0.023 Ω g for the overpotential range: 270–620 mV, correspondingly (i.e. the R_{ct} reduction by 3.6× and 2.3× at 270 mV, and by 2.1× at 620 mV for the Co- and Mo-modified catalyst materials, respectively). Similarly, changing radius of the low-frequency semicircle (adsorption of reaction intermediates response) also resulted in a relatively constant decrease of the R_{Ads} parameter value by *ca*. 8 and 3 times for the cobalt-based, and by 18 and 1.4 times for the Mo-modified Ni foam electrodes, for the overpotentials of 270 and 620 mV.

It has also to be stated that deposition of catalytic Co, and Mo nanostructures (see Fig. 1 in **Paper III**) resulted in a considerable enhancement of the electrochemically accessible surface area. The latter could be easily observed in the cyclic voltammetry plot presented for

the baseline and the Co- and Mo-modified Ni foam materials in Fig. 6 above. Consequently, significant surface modification for the Co- and Mo-modified Ni foams is demonstrated by considerably increased current-density within the corresponding CV profiles. Also, the reported values of the C_{dl} parameter (Table 2 in **Paper III**) at η = 270 mV came to 541,047 μF g^{-1} $s^{\varphi 1-1}$ (Co-modified Ni foam) and 822,987 μF g^{-1} $s^{\varphi 1-1}$ for the Mo-based Ni foam catalyst material, which translates to about 4.5 and 6.8 times augmentation of the electrochemically active surface area values for both catalyst-modified electrodes, in contrast to the baseline, electrooxidized Ni foam anode. Once these surface coefficients are referred to the previously calculated ratios of the R_{ct} parameter, it becomes evident that the cobalt-activated nickel foam anode exhibited superior OER performance.

Table 5 below presents comparison of experimentally recorded here OER parameters for Co-modified Ni foam, derived from electrochemical impedance spectroscopy, with those produced by other authors, at the surfaces of Ni foam baseline material, modified with different catalysts, under analogous experimental conditions. Hence, all the R_{ct} values recorded for the following electrodes: Co-modified Ni foam (**Paper III**), Ni-Ni_3S_2- [72], Ni_2Mo_3N- [73], NiO@Ru- [74] and $CoFe_2O_4$-modified Ni foam materials [75], were comparable at the corresponding overpotentials. However, it should be noticed that these electrochemical examinations [72-75] were carried-out in alkaline solution of much higher concentration (1.0 M KOH vs. 0.1 M NaOH). Interestingly, Co-modified Ni foam anode exhibits radically lower values of the double-layer capacitance parameter, contrary to electrodes presented in other relevant articles (Table 5). Nevertheless, employed procedure (e.g. electrode potential at which the C_{dl} was derived) or unclear determination and employment of electrochemically active surface area to perform calculations by the authors of these works unable to make any

reasonable comparisons to the results obtained on the cobalt-modified nickel foam by the author of this thesis (see Table 5 below and Refs. 72-75 for details).

Table 5 Comparison of the electrochemical parameters for OER derived from electrochemical impedance spectroscopy at the surfaces of Ni foam baseline material modified with different catalysts, under alkaline conditions.

Catalyst material	**Electrolyte**	R_{ct}/Ω	C_{dl}/mF cm^{-2} s$^{\varphi-1}$	η/mV	**Reference**
Co-modified Ni foam	0.1 M NaOH	1.865	1.075	273	This work
		1.004	0.282	370	
Ni-Ni_3S_2 modified Ni foam	1.0 M KOH	1.30	3.0	400	[72]
Ni_2Mo_3N/NF	1.0 M KOH	1.861	347.24	400	[73]
NiO@Ru supported Ni foam	1.0 M KOH	0.66	21.30	400	[74]
$CoFe_2O_4$/NF	1.0 M KOH	2.08	23.29	273	[75]

6.3.Alkaline Water Electrolyser Unit

Additionally, a laboratory scale *ca*. 500 W alkaline water electrolyser unit (see details in **Paper IV**), based on innovative electrode materials and optimized arrangement was fabricated for the purpose of generating hydrogen and oxygen gases of high purity. In the scope of this work, the former gas is commercially important, as:

a) H_2 could be re-electrified in PEM fuel cells,
b) It might be employed as a fuel to produce heat in hydrogen furnaces and
c) It could be further processed to derive industrially important products, such as methane or ammonia.

All electrochemical examinations were performed for both a single-cell unit and electrolyser stack, which combined nine electrochemical cells connected in series, filled with constantly recirculating 8.0 M KOH working electrolyte at *ca*. 45 ºC. Each cell contained two electrodes, placed on the opposite sides, namely: cathode (base Ni foam or Pd-modified Ni foam – *ca.* 0.05-0.10 wt.% of Pd element content) and anode (extensively electrooxidized Ni foam electrode). The distance between the electrodes was practically equal to the thickness of Zirfon Perl UTP 500 membrane (0.5 mm thick), which resulted in significant reduction of the cell's/stack's resistance. Moreover, catalytic performance and durability of the proposed AWE setup were validated, parametrized with experimental data and examined along with purity assessment of the electrolysis products.

Hence, Fig. 8 below presents initial examinations performed on a single-cell in a galvanostatic mode, at current-intensities of 0.5 and 1.0 A. From the dependance of voltage in function of electrolysis time recorded at 0.5 A, it may be concluded that mean values of the cell's voltage oscillated around 1.780 ± 0.005 and 1.647 ± 0.003 V for the base Ni foam and the Pd-activated Ni foam cathodes, correspondingly. When the applied current intensity was raised to 1.0 A, it resulted in elevation of the recorded single-cell electrolyser's voltages to

1.867 ± 0.001 and 1.794 ± 0.009 V, respectively. Moreover, application of surface electro-oxidized Ni foam anode did not lead to any significant improvement of the cell's voltage (compare with similar cell voltages recorded by Zayat et al. in Ref. 76 under analogous experimental conditions, but on low carbon steel-based composite electrodes).

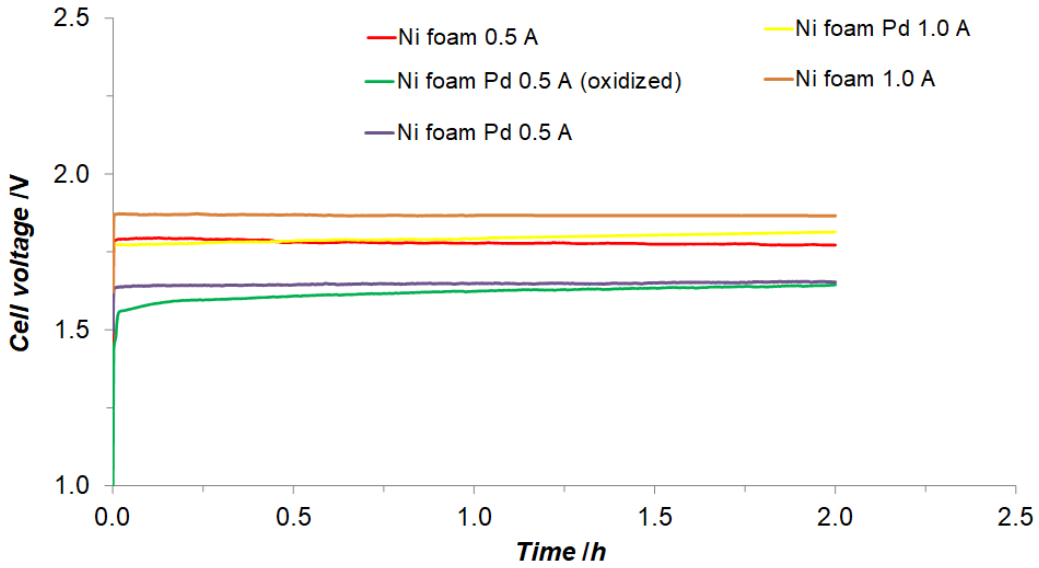


Figure 8 Initial single-cell's voltages as a function of electrolysis time, examined on various electrode setups at 45 ºC in 8.0 M KOH for the employed current-intensities of 0.5 and 1.0 A.

Electrochemical impedance spectroscopy tests (**Paper IV**) were performed on the single-cell electrolyser unit in 8.0 M KOH solution at 45 ºC, over the frequency range of 100 kHz to 1 Hz. The recorded Nyquist impedance plots (Figs. 9a and 9b) exhibited somewhat distorted single semi-circles, which electrochemically could be translated into a charge-transfer reaction (R_{ct} resistance in parallel with electrical double-layer capacitance, C_{dl} parameter).

As expected, the increase of the electrolyser's voltage from 1.50 to 1.80 V resulted in radically reduced total value of the recorded charge-transfer resistance within the cell. Hence, the corresponding R_{ct} parameter diminished from 0.94 to 0.09 Ω and from 0.12 to reach 0.06 Ω, for the cathode made of unmodified and the Pd-activated Ni foam, correspondingly. At the same time, the use of Pd nanoparticle catalyst modification resulted in the total R_{ct} reduction by approximately 30% (from 0.09 to 0.06 Ω) for the maximum value of the cell's voltage (U= 1.80

V). The above corresponds to a *ca*. 4-fold increase (from 96 to 399 mF) of the measured electrical double-layer capacitance parameter. This result could primarily be interpreted as a significant increase in the catalytically active surface of nickel foam cathode, due to the deposition of palladium nanoparticles. Thus, facilitation of the water electrolysis process on Pd-activated Ni foam cathode is a combined effect of: (a) an increase in the electrochemically active electrode surface (measurement of the C_{dl} parameter) and (b) the catalytic properties of Pd nanoparticles in the process of hydrogen evolution. The detailed results on the impedance characteristics of examined in **Paper IV** systems are presented in Table 6 below.

Table 6 Total, average values of charge-transfer resistance and double-layer capacitance parameters, obtained for a single-cell electrolyser unit (anode: Ni foam; cathode: unmodified and Pd-supported Ni foam), recorded in 8.0 M KOH solution at 45 ºC.

***U*/V**	***R*$_{ct}$/Ω**	***C*$_{dl}$/mF**
Cathode: Ni foam		
1.50	0.94	140
1.60	0.58	121
1.65	0.38	113
1.70	0.18	103
1.80	0.09	96
Cathode: Pd-modified Ni foam		
1.50	0.12	669
1.60	0.12	654
1.65	0.11	486
1.70	0.08	450
1.80	0.06	399

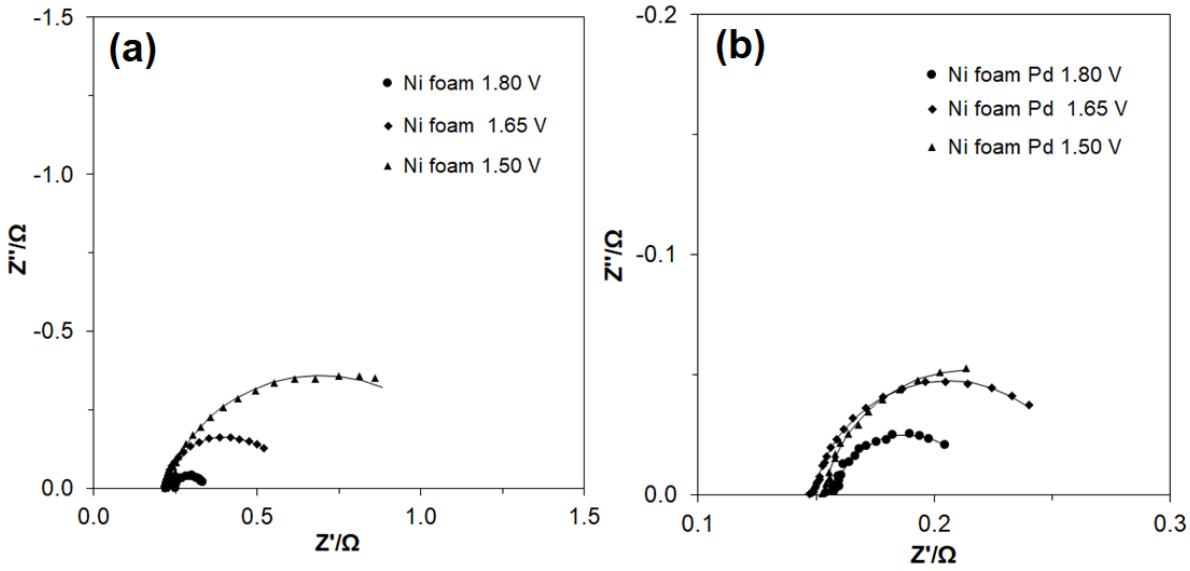


Figure 9 Electrochemical complex-plane impedance Nyquist plots for alkaline water electrolysis process (total impedance measured for a single-cell electrolyser unit), obtained for specified cell voltages, on unmodified (**a**) and palladium-activated Ni foam cathode material (**b**), in contact with 8.0 M KOH at 45 ºC.

Furthermore, this work presents the results of unpublished, single-cell electrochemical tests, performed for two additional electrode sets, namely Ir-modified Ni foam as a cathode and two anodes, i.e. extensively electroodixized and Co-activated nickel foam electrodes. Hence, Fig. 10 below shows the recorded, average cell voltages obtained at current-intensities of 0.5 and 1.0 A for the electrooxidized and cobalt-modified Ni foam anodes. For the current set at 0.5 A, average cell voltages recorded for the oxidized Ni foam and the Co-modified nickel foam anodes reached about 1.690 ± 0.001 V and 1.682 ± 0.003 V, respectively. Furthermore, when the applied current was raised to 1.0 A, the electrolyser's voltages increased to 1.748 ± 0.003 V and 1.760 V ± 0.002 V, correspondingly.

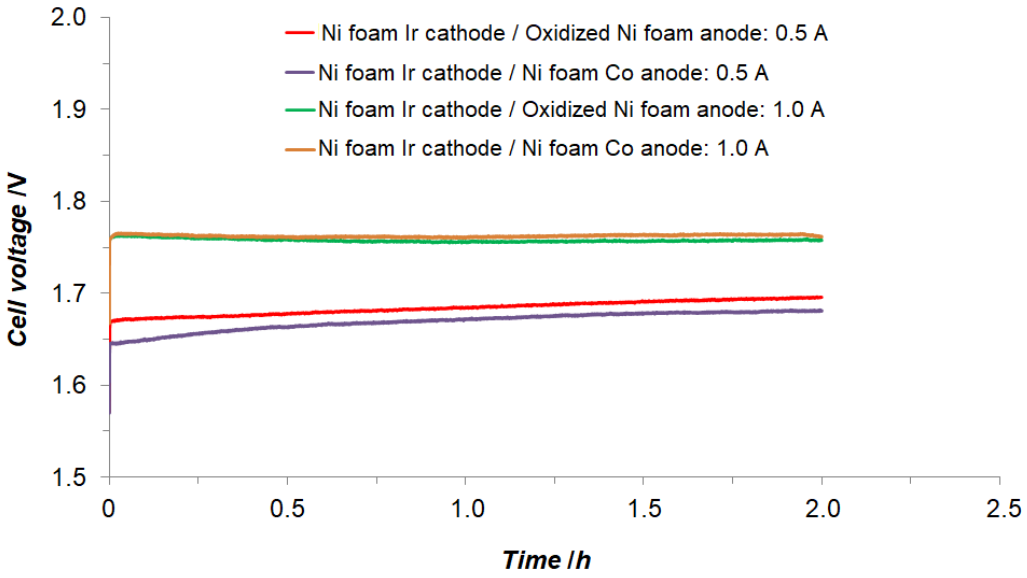


Figure 10 Initial, single-cell's voltages as a function of electrolysis time, examined on indicated electrode configurations in 8.0 M KOH solution, at 45 ºC for the employed current-intensities of 0.5 and 1.0 A.

Additionally, the recorded Nyquist impedance plots are presented in Figs. 11a and 11b (distorted single semi-circles), which could be translated to a total charge-transfer reaction (R_{ct} resistance in parallel with electrical double-layer capacitance, C_{dl}). When the single-cell's voltage was raised from 1.50 to 1.80 V, the recorded total R_{ct} value within the cell became reduced from 0.132 to 0.027 **Ω** and from 0.182 to reach 0.045 **Ω** for the cell composed of Ir-modified Ni foam cathode and Co-modified, and electrochemically oxidized Ni foam anode, respectively (Table 7). The above-described R_{ct} behaviour compares fairly-well with the results presented in **Paper IV**. Furthermore, the recorded C_{dl} parameter exhibited (in both cases) significant reduction along with the increase of the applied cell voltage (see Table 7 again). As already discussed, the latter effect results from gradually increased blocking of electrochemically available electrode surface area by freshly generated gas bubbles.

Table 7 Total, average values of the reaction resistance and double-layer capacitance parameters, obtained for a single-cell electrolyser unit (anode: electrooxidized or Co-modified Ni foam; cathode: Ir-activated Ni foam), recorded in 8.0 M KOH solution at 45 ºC.

U/V	R_{ct}/Ω	C_{dl}/mF
Anode: Oxidized Ni foam		
1.50	0.182	757
1.60	0.095	630
1.65	0.062	630
1.70	0.066	555
1.80	0.045	545
Anode: Co-modified Ni foam		
1.50	0.132	1450
1.60	0.120	320
1.65	0.065	232
1.70	0.049	212
1.80	0.027	173

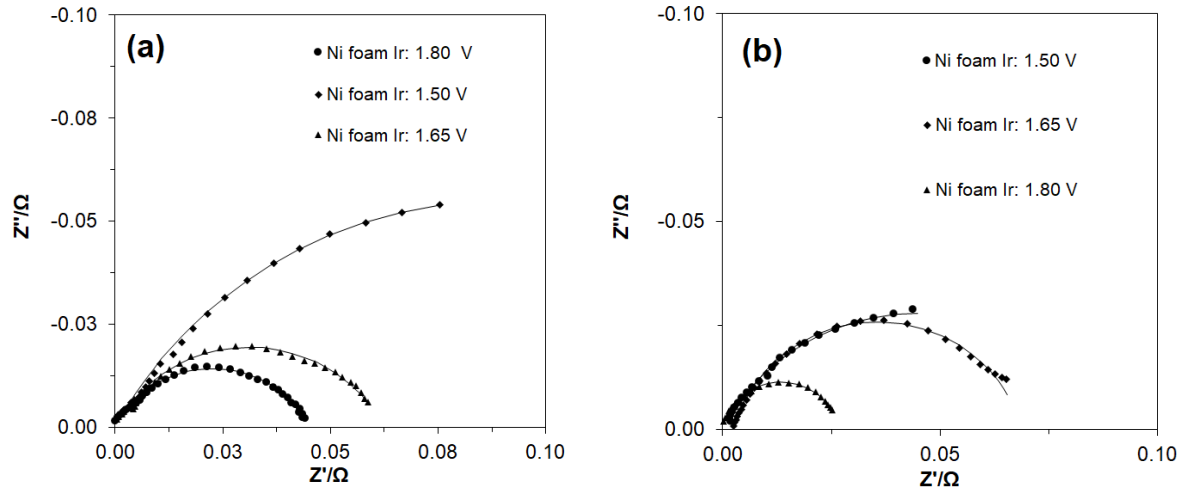


Figure 11 Electrochemical complex-plane impedance Nyquist plots for alkaline water electrolysis process (total impedance measured for a single-cell electrolyser unit), obtained for specified cell voltages, on Ir-modified Ni foam cathode with electrooxidized Ni foam (**a**) and cobalt-activated Ni foam anode materials (**b**), in contact with 8.0 M KOH at 45 ºC.

Then, operational stability of the proposed, single-cell electrolyser arrangements was examined during continuous, 24-hour galvanostatic mode (applied current was set at 1.0 A) experiments. Hence, from the dependance of the recorded voltage in function of electrolysis time, it may be concluded that mean values of the cell's voltage reached *ca.* 1.791 ± 0.008 and

1.775 ± 0.006 V, correspondingly for the electrooxidized and the Co-modified Ni foam anodes. The cell's voltage parameter remained stable over the 24-hour period (see Fig. 12**)**.

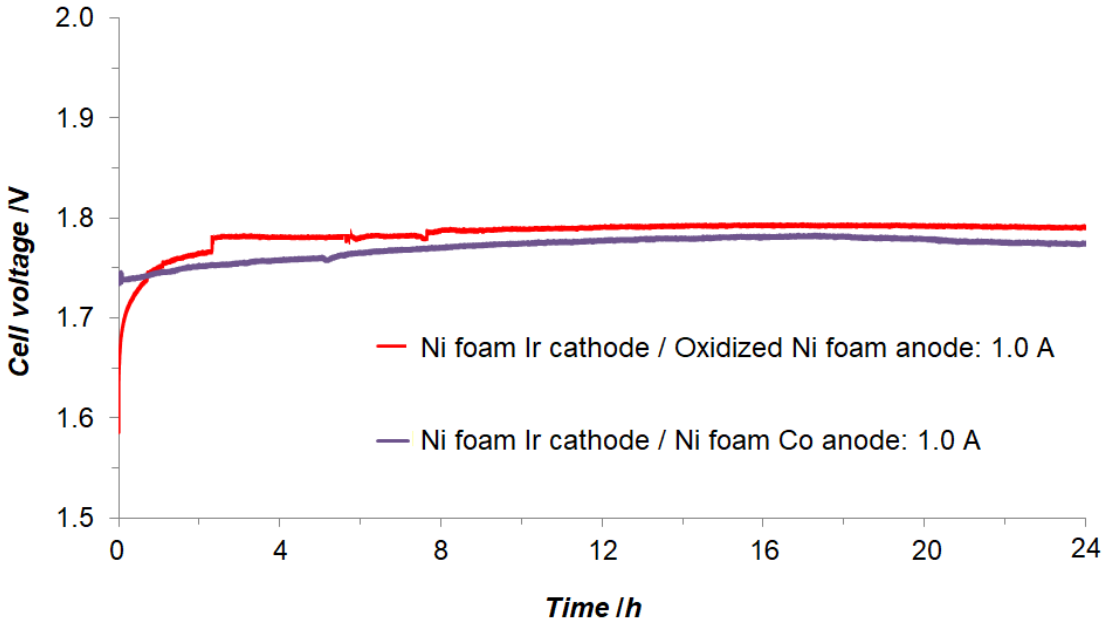


Figure 12 Single-cell's electrolyser voltage in function of electrolysis time during long-time, 24-hour examination, recorded for two anode arrangements. The electrolysis process was carried-out at 45 ºC in 8.0 M KOH supporting solution for the set current of 1.0 A, for electrooxidized and Co-supported Ni foam anodes. The solution was constantly recirculated at the rate of 50 cm^3 min^{-1}.

Finally, a technical scale, multi-cell electrolyser stack with a nominal power of *ca*. 500 W was also assembled and tested under operating laboratory fume-hood (see Fig. 2 in **Paper IV**), where two silica gel-filled columns were employed for drying hydrogen and oxygen gas products.

Hence, for the galvanostatic AWE experiments (see Fig. 13 below) carried out at the current intensity of 1.0 A and the duration of 24 hours, the recorded average, steady voltages of the electrolyser stack came respectively to 16.22 ± 0.02 and 15.86 ± 0.04 V for unmodified and the Pd-activated Ni foam cathodes. In the latter case, there was a tendency of voltage increase from 15.60 ± 0.03 to 15.93 ± 0.08 V (over the period of 24 hours), which could be caused by slow deactivation of Pd catalytic sites (see Fig. 13a). Then, the increase of the current intensity to 3.5 A caused elevation of the average voltage of the electrolyser to 17.73 and 17.40

V, respectively. In this case, a small voltage rise (from 17.26 to 17.52 V) was also observed for the Pd-modified nickel foam cathodes. Furthermore, for the current set at 16.0 A, average recorded voltages of the electrolyser came to 22.21 ± 0.03 V (for unmodified cathodes) and 22.03 ± 0.04 V for the Pd-modified Ni foam electrodes (Fig. 13b).

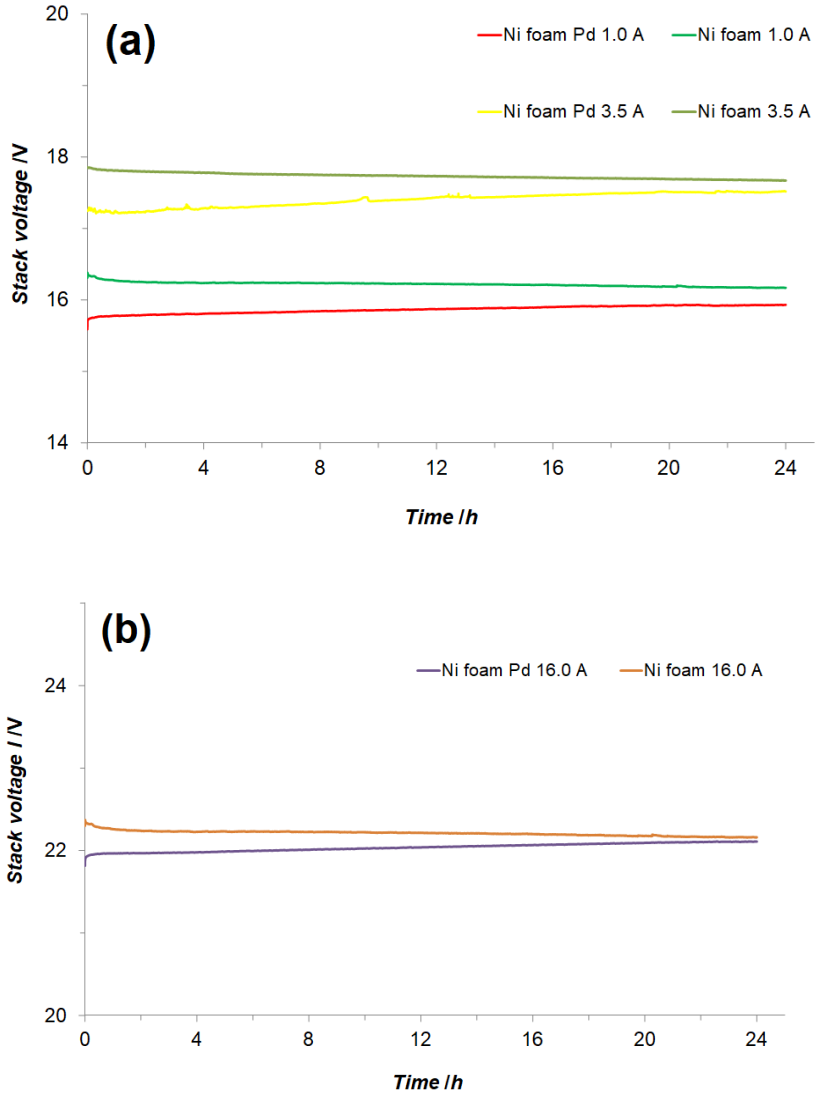


Figure 13 Electrolyser stack's voltage in function of electrolysis time over a 24-hour period, examined at 45 ºC in 8.0 M KOH for the applied current intensities of 1.0 and 3.5 A (**a**) and 16.0 A (**b**), for Ni foam anode, pure Ni foam and Pd-activated Ni foam cathodes.

Finally, in order to confirm the stability and the assumed device's power of approximately 500 W, extended (7-day long) water electrolysis tests were also carried out for

both cathode arrangements. Initially, the current was set at 23.6 A (Pd-activated Ni foam) and 21.0 A for the unmodified nickel foam electrode systems. Hence, after approximately 130 hours of continuous electrolyser operation, the voltages for both tested cathode systems (*ca*. 23.83 V: Ni foam/Pd and 23.86 V: Ni foam or 2.65 V/cell) became practically equilibrated. At this point, the tested AWE unit stacks reached the power of 501 and 562 W for the unmodified and the Pd-activated Ni foam electrodes, correspondingly. Simultaneously, the obtained results indicated minor, but visible, deactivation effect for the palladium-modified cathodes. The latter effect most likely results from deposition/electrosorption of electrolyte trace pollutants on the Pd-modified cathode surface (for the unmodified cathode system, the voltage changes are even less significant, Fig. 14).

During a long-time continuous operation of the AWE system, freshly generated H_2 and O_2 gases were collected in four different time intervals. Then, samples of both gases were analyzed by means of a GC technique (see detailed description in **Paper IV**). Their compositions are illustrated in Table 8 below. Thus, an average purity of four oxygen samples came to 99.59%, whereas that of hydrogen (also calculated as an average of four samples) approached 99.88%. The former gas was mainly polluted with trace amounts of H_2O and H_2, whereas the latter one was contaminated with very trace amounts of H_2O.

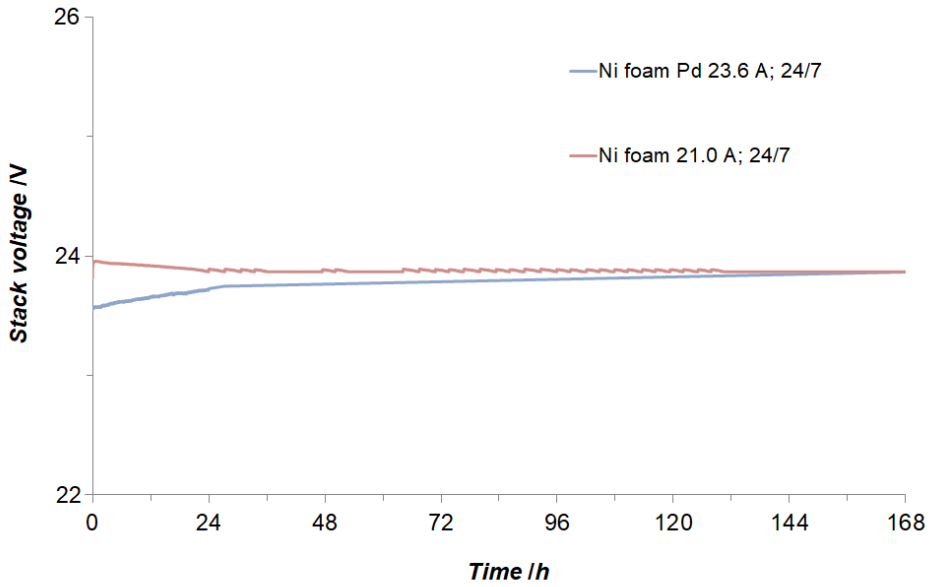


Figure 14 Electrolyser stack's voltage in function of electrolysis time during long-term (7 days) examinations recorded for two cathode arrangements. The electrolysis process was executed at 45 ºC in 8.0 M KOH supporting solution for the set current intensities of 21.0 and 23.6 A for pure Ni foam and Pd-activated Ni foam cathodes, correspondingly. The solution was constantly recirculated at the rate of 50 cm^3 min^{-1}.

Table 8 Chromatograhpic analysis of H_2 and O_2 gas samples generated during the continuous operation of 500 W AWE stack.

Sample	Constituents	Content [%]
Oxygen 1	O_2	99.83
	H_2O	0.17
Oxygen 2	O_2	98.71
	H_2	1.11
	H_2O	0.18
Oxygen 3	O_2	99.96
	H_2O	0.04
Oxygen 4	O_2	99.87
	H_2O	0.13
Hydrogen 1	H_2	99.86
	H_2O	0.14
Hydrogen 2	H_2	99.85
	H_2O	0.15
Hydrogen 3	H_2	99.94
	H_2O	0.06
Hydrogen 4	H_2	99.89
	H_2O	0.11

7. Conclusions

1. Employed surface chemical/electrochemical pre-treatments of Ni foam base electrode resulted in a radical expansion (by *ca.* 6 times vs. unmodified Ni foam material at the cathodic overpotential of 100 mV) of electrochemically accessible surface area of the Ni foam baseline material. Such surface then becomes catalytic for its further modification by highly homogeneous, nanoparticle, noble metal deposits.
2. Modification of the baseline Ni foam material *via* electrodeposition or spontaneous deposition of iridium nanoparticles at sub percent Ir levels resulted in a radically improved catalytic activity (with j_0 values increased by *ca*. 3.3 to 14.4 times vs. etched Ni foam material) of such-produced nickel composites towards cathodic hydrogen generation (HER).
3. Laboratory produced Ni foam-based materials allowed successful fabrication of a sub-technical scale alkaline ~500 W water electrolyser unit, which then indicated substantial opportunities for this type of cathode (also anode) materials in industrial AWE systems.
4. Catalytic modification of Ni foam by means of electrochemical deposition of transition metals nanoparticles (namely cobalt and molybdenum) at very low surface loadings allowed for significant activity improvement (with j_0 values increased by *ca.* 986 and 1352 times for Co- and Mo-activated Ni foam, respectively vs. baseline Ni foam electrode, measured at the anodic overpotential of 370 mV) of the base Ni foam material towards anodic evolution of oxygen (OER).
5. Extended electrooxidation of the Ni foam base material provided relatively low electrochemical OER performance, being most likely a result of gradual development of thick and poorly conductive nickel oxide layer.
6. Laboratory size alkaline water electrolysis (AWE) experiments, performed on Pd-modified Ni foam cathodes, revealed a well-suited, *ca*. 500 W electrolyser unit with enhanced

electrochemical performance (examined AWE unit stacks reached the power of 501 and 562 W for the unmodified and the Pd-supported Ni foam electrodes, respectively, when the current was set at 21.0 A and 23.6 A for the corresponding electrode systems), high-purity H_2 and O_2 gas products, and high electrode stability during its 7-day long operation.

7. Single-cell electrolyser unit comprising Ir-modified Ni foam cathode and Co-activated nickel foam anode, revealed enhanced electrochemical performance vs. Ni foam/Ir cathode and electrooxidized Ni foam anode (total, average value of the reaction resistance, recorded for the cell voltage of 1.5 V, was reduced by 1.4 times, when the capacitance parameter was simultaneously diminished by *ca.* 1.9 times). Moreover, both single-cell systems exhibited high electrode stability during their 24-hour continuous operation.
8. Further laboratory work is required in order to optimize the electrolyser's operational parameters (including: electrolyte composition, recirculation rate and temperature, and maximum operational voltage) along with the stack's engineering.

Future Perspectives

My future research plans aim at continuation of research activities related to applied electrochemistry, especially to electrochemical generation of hydrogen and oxygen gases (AWE systems), utilizing innovative baseline materials (e.g. carbon fibre or graphene foam) along with novel HER, and OER catalytic nanoparticle combinations and electrolyser designs.

References

1. Marks-Bielska, R.; Bielski, S.; Pik, K.; Kurowska, K. The Importance of Renewable Energy Sources in Poland's Energy Mix. *Energies*, **2020**, 13, 1-23.
2. Perera, F. Pollution from Fossil-Fuel Combustion is the Leading Environmental Threat to Global Pediatric Health and Equity: Solution Exist. *International Journal of Environmental Research and Public Health*. **2018**, 15, 1-17.
3. Ahmad, T.; Zhang, D. A critical review of comparative global historical energy consumption and future demand: The story told so far. *Energy Reports*, **2020**, 6, 1973-1991.
4. Hunt, N.D.; Liebman, M.; Thakrar, S.K.; Hill, J.D. Fossil Energy Use, Climate Change Impacts, and Air Quality-Related Human Health Damages of Conventional and Diversified Cropping Systems in Iowa, USA. *Environmental Science & Technology*. **2020**, 54, 11002-11014.
5. Owusu, P.A.; Asumadu-Sarkodie, S. A review of renewable Energy sources, sustainability issues and climate change mitigation. *Cogent Engineering*. **2016**, 3, 1-14.
6. Panwar, N.L.; Kaushik, S.C.; Kothari, S. Role of renewable energy sources in environmental protection: A review. *Renewable and Sustainable Energy Reviews*. **2011**, 15, 1513-1524.
7. Bounocore, J.J.; Hughes, E.J.; Michanowicz, D.R.; Heo, J.; Allen, J.G.; Williams, A. Climate and health benefits of increasing renewable energy deployment in the USA. *Environmental Research Letters*. **2019**, 14, 1-14.
8. Halkos, G.E.; Gkampoura, E.-C. Reviewing Usage, Potentials, and Limitations of Renewable Energy Soures. *Energies*. **2020**, 13, 1-19.
9. Hayat, M.B.; Ali, D.; Monyake, K.C.; Alagha, L.; Ahmed, N. Solar energy – A look into power generation, challenges, and a solar-powered future. *International Journal of Energy Research* **2019**, 43, 1049-1067.
10. Mostafaeipour, A.; Alvandimanesh, M.; Najafi, F.; Issakhov, A. Identifying challenges and barriers for development of solar energy by using fuzzy best-worst method: A case study. *Energy*. **2021**, 226, 1-22.
11. Firestone, J.; Hoen, B.; Rand, J.; Elliott, D.; Hubner, G.; Pohl, J. Reconsidering barriers to wind power projects: community engagement, developer transparency and place. *Journal of Environmental Policy & Planning*. **2018**, 20, 370-386.
12. Nikolaidis, P.; Poullikkas, A. A comparative review of electrical energy storage systems for better sustainability. *Journal of Power Technologies*. **2017**, 97, 220-245.
13. Kousksou, T.; Bruel, P.; Jamil, A.; El Rhafiki, T.; Zeraouli, Y. Energy storage: Applications and challenges. *Solar Energy Materials & Solar Cells*. **2014**, 120, 59-80.
14. Wang, M.; Wang, G.; Sun, Z.; Zhang, Y.; Xu, D. Review of renewable energy-based hydrogen production processes for sustainable energy innovation. *Global Energy Interconnection*. **2019**, 2, 436-443.
15. Hosseini, S.E.; Wahid, M.A. Hydrogen production from renewable and sustainable energy resources: Promising green energy for clean development. *Renewable and Sustainable Energy Reviews.* **2016**, 57, 850-866.
16. Kotowicz, J.; Jurczyk, M.; Węcel, D.; Ogulewicz, W. Analysis of hydrogen production in alkaline electolyzers. *Journal of Power Technologies.* **2016**, 96, 149-156.

17. Staffel, I.; Scamman, D.; Abad, A.V.; Balcombe, P.; Dodds, P.E.; Ekins, P.; Shah, N.; Ward, K.R. The role of hydrogen and fuel cells in the global energy system. *Energy & Environmental Science*. **2019**, 12, 1-29.
18. Abdalla, A.M.; Hossain, S.; Nisfindy, O.B.; Azad, A.T.; Dawood, M.; Azad, A.K. Hydrogen production, storage, transportation and key challenges with applications: A review. *Energy Conversion and Management*. **2018**, 165, 602-627.
19. Hwang, H.T.; Varma, A. Hydrogen storage for fuel cell vehicles. *Current Opinion in Chemical Engineering*. **2014**, 5, 42-48.
20. Kakaoulaki, G.; Kougias, I.; Taylor, N.; Dolci, F.; Moya, J.; Jager-Waldau, A. Green hydrogen in Europe – A regional assessment: Substituting existing production with electrolysis powered by renewables. *Energy Conversion and Management*. **2021**, 228, 1-19.
21. Momirlan, M.; Veziroglu, T.N. The properties of hydrogen as fuel tomorrow in sustainable energy system for a cleaner planet. *International Journal of Hydrogen Energy*. **2005**, 30, 795-802.
22. Idriss, H.; Scott, M.; Subramani, V. 1 – Introduction to hydrogen and its properties. In *Compedium of Hydrogen Energy*; Subramani, V.; Basile, A.; Nejat Veziroglu, T. Woodhead Publishing: Sawston, UK, 2015; Volume 1, pp. 3-19.
23. Rivard, E.; Trudeau, M.; Zaghib, K. Hydrogen Storage for Mobility: A Review. *Materials*. **2019**, 12, 1-22.
24. Ni, M.; An Overview of Hydrogen Storage Technologies. *Energy Exploration & Exploitation*. **2006**, 24, 197-209.
25. Eller, J.; Sauerborn, T.; Becker, B.; Buntic, I.; Gross, J.; Helmig, R. Modeling Subsurface Hydrogen Storage With Transport Properties From Entropy Scaling Using the PC-SAFT Equation of State. *Water Resources Research*. **2022**, 58, 1-19.
26. Kreith, F.; West, R. Fallacies of a Hydrogen Economy: A Critical Analysis of Hydrogen Production and Utilization. *Journal of Energy Resources Technology*. **2004**, 126, 249-257.
27. Song, J.; Zhang, C.; Lin, G.; Zhang, Q. Performance and emission of an electronic control common-rail diesel engine fuelled with liquefied natural gas-diesel dual-fuel under an optimization control scheme. *Proceedings of the Institution of Mechanical Engineers, Part D: Journal of Automobile Engineering* **2019**, 223, 1-11.
28. Ferriday, T.B.; Middleton, P.H.; Kolhe, M.L. Review of the Hydrogen Evolution Reaction – A Basic Approach. *Energies*, **2021**, 14, 1-43.
29. Li, D.; Zhang, B.; Li, Y.; Chen, R.; Hu, S.; Ni, H. Boosting hydrogen evolution activity in alkaline media with dispersed ruthenium clusters in NiCo-layered double hydroxide. *Electrochemistry Communications*. **2019**, 101, 23-27.
30. Durovic, M.; Hnat, J.; Bouzek, K. Electrocatalysts for the hydrogen evolution reaction in alkaline and neutral media. A comparative review. *Journal of Power Sources*. **2021**, 493, 1-17.
31. Wang, S.; Lu, A.; Zhong, C.-J. Hydrogen production from water electrolysis: role of catalysts. *Nano Convergence*. **2021**, 8, 1-23.
32. Zheng, Y.; Jiao, Y.; Vasileff, A.; Qiao, S.-Z. The Hydrogen Evolution Reaction in Alkaline Solution: From Theory, Single Crystal Models, to Practical Electrocatalysts. *Journal of the German Chemical Society*. **2018**, 57, 1-12.

33. Tang, L.; Yu, J.; Zhang, Y.; Tang, Z.; Qin, Y. Boosting the hydrogen evolution reaction activity of Ru in alkaline and neutral media by accelerating water dissociation. *RSC Advances*. **2021**, 11, 1-7.
34. Baek, D.S.; Lee, J.; Lim, J.S.; Joo, S.H. Nanoscale electrocatalyst design for alkaline hydrogen evolution reaction through activity descriptor identification. *Materials Chemistry Frontiers*. **2021**, 5, 1-17.
35. Jamesh; M.-I. Sun, X. Recent progress on earth abundant electrocatalysts for oxygen evolution reaction (OER) in alkaline medium to achieve efficient water splitting – A review. *Journal of Power Sources*. **2018**, 400, 31-68.
36. Liang, Q.; Brocks, G.; Bieberle-Hutter, A. Oxygen evolution reaction (OER) mechanism under alkaline and acidic conditions. *Journal of Physics: Energy*. **2021**, 3, 1-7.
37. Plevova, M.; Hnat, J.; Bouzek, K. Electrocatalysts for the oxygen evolution reaction in alkaline and neutral media. A comparative review. *Journal of Power Sources*. **2021**, 507, 1-16.
38. Divanis, S.; Kutlusoy, T.; Ingmer Boye, I.M.; Man, I.C.; Rossmeisl, J. Oxygen evolution reaction: a perspective on a decade of atomic scale simulations. *Chemical Science*. **2020**, 11, 1-8.
39. Suen, N.-T.; Hung, S.-F.; Quan, Q.; Zhang, N.; Xu, Y.-J.; Chen, H.M. Electrocatalysis for the oxygen evolution reaction: recent development and future perspectives. *Chemical Society Reviews*. **2017**, 46, 337-365.
40. Habekost, A. Fundamentals and Applications of Electrochemical Impedance Spectroscopy – A Didactic Perspective. *World Journal of Chemical Education*. **2021**, 9, 14-21.
41. Lasia, A. Definition of Impedance and Impedance of Electrical Circuits. In. *Electrochemical Impedance Spectroscopy and its Applications*. Ed. 2; Springer: Berlin/Heidelberg, Germany, 2014; pp. 7-64.
42. Meddings, N.; Heinrich, M.; Overney, F.; Lee, J.-S.; Ruiz, V.; Napolitano, E.; Seits, S.; Hinds, G.; Raccichini, R.; Gaberscek, M.; Park, J. Application of electrochemical impedance spectroscopy to commercial Li-ion cells: A review. *Journal of Power Sources*. **2020**, 480, 1-27.
43. Magar, H.S.; Hassan, R.Y.A.; Mulchandani, A. Electrochemical Impedance Spectroscopy (EIS): Principles, Construction, and Biosensing Applications. *Sensors*. **2021**, 21, 1-21.
44. Wang, S.; Zhang, J.; Gharbi, O.; VIvier, V.; Gao, M.; Orazem, M.E. Electrochemical Impedance Spectroscopy. *Nature Reviews Methods Primers*. **2021**, 1, 1-21.
45. Elgrishi, N.; Rountree, K.J.; McCarthy, B.D.; Rountree, E.S.; Eisenhart, T.T.; Dempsey, J.L. A Practical Beginner's Guide to Cyclic Voltammetry. *Journal of Chemical Education*. **2018**, 95, 197-206.
46. Espinoza, E.M.; Clark, J.A.; Soliman, J.; Derr, J.B.; Morales, M.; Vullev, V.I. Practical Aspects of Cyclic Voltammetry: How to Estimate Reduction Potentials When Irreversibility Prevails. *Journal of The Electrochemical Society*. **2019**, 166, 1-14.
47. Seri, O.; Siree, B. The Differentiating Polarization Curve Technique for the Tafel Parameter Estimation. *Catalysts*. **2017**, 7, 1-15.

48. Khadke, P.; Tichter, T.; Boettcher, T.; Muench, F.; Ensiger, W.; Roth, C. A simple and effective method for the accurate extraction of kinetic parameters using differential Tafel plots. *Scientific Reports.* **2021**, 11, 1-15.
49. Moropoulou, A.; Zendri, E.; Ortiz, P.; Delegou, E.T.; Ntoutsi, I.; Balliana, E.; Becerra, J.; Ortiz, R. Scanning Microscopy Techniques as an Assessment Tool of Materials and Interventions for the Protection of Built Cultural Heritage. *Scanning*. **2019**, 11-12, 1-20.
50. Raval, N.; Maheshwari, R.; Kalyane, D.; Youngren-Ortiz, S.R.; Chougule, M.B.; Tekade, R.T. Chapter 10 – Importance of Physicochemical Characterization of Nanoparticles in Pharmaceutical Product Development. In *Basic Fundamentals of Drug Delivery*, Tekade, R.K. Academic Press: Cambridge, US, **2019**; pp. 369-400.
51. Brodush, N.; Brahimi, S.V.; De Melo, E.B.; Song, J.; Yue, S.; Piche, N.; Gauvin, R. Scanning Electron Microscopy versus Transmission Electron Microscopy for Material Characterization: A Comparative Study on High-Strength Steels. *Scanning*. **2021**, 4, 1-19.
52. Khan, M.S.I.; Oh, S.-W.; Kim, Y.-J. Power of Scanning Electron Microscopy and Energy Dispersive X-Ray Analysis in Rapid Microbial Detection and Identification at the Single Cell Level. *Scientific Reports*. **2020**, 10, 1-10.
53. Bergstrom, J. 2 – Experimental Characterization Techniques. In. *Mechanics of Solid Polymers*. William Andrew: Norwich, US, **2015**; pp. 19-114.
54. Ebnesajjad, S. Chapter 4 – Surface and Material Characterization Techniques. In. *Surface Treatment of Materials for Adhesive Bonding*. 2nd ed.; Ebnesajjad, S. William Andrew Publishing: Norwich, US, **2014**, pp. 39-75.
55. Scimeca, M.; Bischetti, S.; Lamsira, H.K.; Bonfiglio, R.; Bonnano, E. Energy Dispersive X-ray (EDX) microanalysis: A powerful tool in biomedical research and diagnosis. *European Journal of Histochemistry*. **2018**, 62, 1-10.
56. Lorenzo, M.; Pico, Y. Chapter 2 – Gas Chromatography and Mass Spectroscopy Techniques for the Detection of Chemical Contaminants and Residues in Foods. In. *Chemical Contaminants and Residues in Foods*., 2nd ed.; Schrenk, D.; Cartus, A. Woodhead Publishing: Sawston, UK, **2017**, pp. 15-50.
57. Marriott, P.J. Chapter 8 Gas chromatography. In. *Journal of Chromatography Library.* 6th ed.; Heftmann, E. Elsevier: Amsterdam, Nerherlands, **2004**; 69, pp. 319-368.
58. He, B.; Kuang, Y.; Hou, Z.; Zhou, M.; Chen, X. Enhanced electrocatalytic hydrogen activity of nickel foam by low-temperature oxidation. *Journal of Materials Research* **2018**, 33, 213-224.
59. Kovalenko, V.; Kotok, V.; Kovalenko, I. Activation of the nickel foam as a current collector for publication in super-capacitors. *Eastern-European Journal of Enterprise Technologies*, **2018**, 93, 1-7.
60. Sikora, E.; Macdonald, D.D. Nature of the passive film on nickel. *Electrochimica Acta*. **2002**, 48, 69-77.
61. Malaie, K.; Heydari, Z.; Brousse, T. Methods – On the Reliability of the Electrochemical Data Recorded on Nickel Foam in Alkaline Solution: The Illusive Surface Oxide Layer. *Journal of the Electrochemical Society*. **2021**, 168, 1-15.
62. Bidauls, F.; Brett, D.J.L.; Middleton, P.H.; Abson, N.; Brandon, N.P. A new application for nickel foam in alkaline fuel cells. *International Journal of Hydrogen Energy*. **2009**, 34, 6799-6808.

63. Pierozynski, B.; Mikolajczyk, T.; Kowalski, I.M. Hydrogen evolution at catalytically-modified nickel foam in alkaline solution. *Journal of Power Sources*. **2014**, 271, 231-238.
64. Pierozynski, B.; Mikolajczyk, T. Cathodic Evolution of Hydrogen on Platinum-Modified Nickel Foam Catalyst. *Electrocatalysis*. **2016**, 7, 121-126.
65. Liu, H.; Ma, X.; Rao, Y.; Liu, Y.; Liu, J.; Wang, L.; Wu, M. Heteromorphic NiCo2S4/Ni3S2/Ni Foam as a Self-Standing Electrode for Hydrogen Evolution Reaction in Alkaline Solution. *ACS Applied Materials & Interfaces.* **2018**, 10, 1-31.
66. Gao, Y.; Wu, Y.; He, H.; Tan, W. Potentiostatic electrodeposition of Ni-Se-Cu on nickel foam as an electrocatalyst for hydrogen evolution reaction. *Journal of Colloid and Interface Sciences*. **2020**, 578, 555-564.
67. Lofti, N.; Shahrabi, T.; Yaghoubinezhad, Y.; Darband, Gh. B. Surface modification of Ni foam by the dendrite Ni-Cu electrode for hydrogen evolution reaction in an alkaline solution. *Journal of Electroanalytical Chemistry.* **2019**, 848, 1-10.
68. Toghraei, A.; Shahrabi, T.; Darband, Gh. B. Electrodeposition of self-supported Ni-Mo-P film on Ni foam as an affordable and high-performance electrocatalyst toward hydrogen evolution reaction. *Electrochimica Acta*. **2020**, 335, 1-9.
69. Xing, J.; Zou, Z.; Guo, K.; Xu, C. The effect of phosphating time on the electrocatalytic activity of nickel phosphide nanorod arrays grown on Ni foam. *Journal of Materials Research* **2018**, 33, 556-567.
70. Conway, B.E.; Pierozynski, B. A.c. impedance behaviour of processes involving adsorption and reactivity of guanidonium-type cations at Pt(100) surface. *Journal of Electroanalytical Chemistry.* **2008**, 622, 10-14.
71. van Drunen, J.; Pilapil, B.K.; Makonnen, Y.; Beauchemin, D.; Gates, B.D.; Jerkiewicz, G. Electrochemically Active Nickel Foams as Support Materials for Nanoscopic Platinum Electrodes. *ACS Applied Materials & Interfaces* **2014**, 6, 12046-12061.
72. Chaudhari, N.K.; Oh, A.; Sa, Y.J.; Jin, H.; Baik, H.; Kim, S.G.; Lee, S.J.; Joo, S.H.; Lee, K. Morphology controlled synthesis of 2-D Ni-Ni3S2 and Ni3S2 nanostroctures on Ni foam towards oxygen evolution reaction. *Nano Convergence*. **2017**, 4, 1-9.
73. Park, S.H.; Kang, S.H.; Youn, D.H. Direct One-Step Growth of Bimetallic Ni_2Mo_3N on Ni Foam as an Efficient Oxygen Evolution Electrocatalysts. *Materials*. **2021**, 14, 1-10.
74. Zhang, L.; Hu, Z.; Li, H.; Ren, Q.; Qiu, Y.; Qu, J.; Hu, S. Nickel Foam Supported NiO@Ru Heterostructure towards High-Efficiency Overall Water Splitting. *ChemPhysChem* **2021**, 22, 1-8.
75. Zhu, S.; Lei, J.; Qin, Y.; Zhang, L.; Lu, L. Spinel oxide $CoFe_2O_4$ grown on Ni foam as an efficient electrocatalyst for oxygen evolution reaction. *RSC Advances* **2019**, 9, 13269-13274.
76. Zayat, B.; Mitra, D.; Narayanan, S.R. Inexpensive and Efficient Alkaline Water Electrolyzed with Robust Steel-Based Electrodes. *Journal of the Electrochemical Society*. **2020**, 167, 1-8.

List of Tables and Figures

Figure 1 Triangular-shaped voltage sweep pattern in cyclic voltammetry technique. 17
Figure 2 Complex-plane impedance plots for HER, carried out on fresh (*as received*) and etched Ni foam electrode surfaces **(a)** in contact with 0.1 M NaOH, recorded at 298 K for the potential of −100 mV (vs. RHE); **(b)** As above, but recorded on Ir-activated Ni foam electrodes via electrodeposition of iridium (ED 1 and ED 2 samples) and spontaneous deposition of Ir (SD 1 electrode). 26
Figure 3 Quasi-steady-state potentiostatic cathodic Tafel polarization curves (recorded at a scan-rate of 0.5 mV s^{-1}) for etched Ni foam, ED1 and SD1 electrodes, carried out in 0.1 M NaOH solution. 28
Figure 4 (a) Cyclic voltammograms recorded for pure, electrochemically oxidized and Pt-modified Ni foam electrodes in contact with 0.1 M NaOH (at 20 ºC), carried-out at a sweep-rate of 50 mV s^{-1}; (**b)** As in (a) above, but recorded for pure and electrochemically oxidized (carried-out by potential hold at 1.8 V/RHE for 30 minutes) Ni foam electrodes. 30
Figure 5 Linear plots of –log R_{ct} vs. T^{-1} for OER on pure and Pt-activated Ni foam electrode surfaces in 0.1 M NaOH solution, carried-out at the potential of 1.5 V. 34
Figure 6 Cyclic voltammogram curves of oxidized, pure Ni, Co- and Mo-activated Ni foam electrodes, in contact with 0.1 M NaOH medium (at 20 °C), carried-out at a scan-rate of 50 mV s^{-1} for the potential span 1.2–1.9 V. 36
Figure 7 Electrochemical impedance Nyquist plots for OER on oxidized Ni foam, Co- and Mo-modified Ni foam electrode surfaces in contact with 0.1 M NaOH, at 20 ºC for the potential of 1.6 V vs. RHE. 37
Figure 8 Initial single-cell's voltages as a function of electrolysis time, examined on various electrode setups at 45 ºC in 8.0 M KOH for the employed current-intensities of 0.5 and 1.0 A. 42
Figure 9 Electrochemical complex-plane impedance Nyquist plots for alkaline water electrolysis process (total impedance measured for a single-cell electrolyser unit), obtained for specified cell voltages, on unmodified (**a**) and palladium-activated Ni foam cathode material (**b**), in contact with 8.0 M KOH at 45 ºC. 44
Figure 10 Initial, single-cell's voltages as a function of electrolysis time, examined on indicated electrode configurations in 8.0 M KOH solution, at 45 ºC for the employed current-intensities of 0.5 and 1.0 A. 45
Figure 11 Electrochemical complex-plane impedance Nyquist plots for alkaline water electrolysis process (total impedance measured for a single-cell electrolyser unit), obtained for specified cell voltages, on Ir-modified Ni foam cathode with electrooxidized Ni foam (**a**) and cobalt-activated Ni foam anode materials (**b**), in contact with 8.0 M KOH at 45 ºC. 46
Figure 12 Single-cell's electrolyser voltage in function of electrolysis time during long-time, 24-hour examination, recorded for two anode arrangements. The electrolysis process was carried-out at 45 ºC in 8.0 M KOH supporting solution for the set current of 1.0 A, for electrooxidized and Co-supported Ni foam anodes. The solution was constantly recirculated at the rate of 50 cm^3 min^{-1}. 47
Figure 13 Electrolyser stack's voltage in function of electrolysis time over a 24-hour period, examined at 45 ºC in 8.0 M KOH for the applied current intensities of 1.0 and 3.5 A (**a**) and 16.0 A (**b**), for Ni foam anode, pure Ni foam and Pd-activated Ni foam cathodes. 48
Figure 14 Electrolyser stack's voltage in function of electrolysis time during long-term (7 days) examinations recorded for two cathode arrangements. The electrolysis process was executed at 45 ºC in 8.0 M KOH supporting solution for the set current intensities of 21.0 and 23.6 A for pure Ni foam and Pd-activated Ni foam cathodes, correspondingly. The solution was constantly recirculated at the rate of 50 cm^3 min^{-1}. 50

Table 1 Electrochemical parameters (with their standard deviations) obtained for HER, recorded on Ni foam (as received and etched) and Ir-modified (spontaneously deposited: SD 1 and SD 2, and electrodeposited: ED 1 and ED 2) Ni foam electrodes in contact with 0.1 M NaOH. 24
Table 2 Comparison of the electrochemical parameters for HER derived from electrochemical impedance spectroscopy technique at the surfaces of Ni foam baseline surface, modified with different catalyst materials, examined under alkaline conditions. 27
Table 3 Comparison of the electrochemical parameters for HER, obtained through Tafel polarization plots at the surfaces of different catalyst materials, under alkaline conditions. 28
Table 4 Electrochemical resistance and capacitance parameters for OER, obtained on fresh, electrooxidized and Pt-activated Ni foam electrodes in contact with 0.1 M NaOH, at 20 ^{o}C (reproducibility about 10-15 %, $\chi^2 = 7\times10^{-5}$ to 4×10^{-4} and 1×10^{-3} for the potential of 1.9 V). 33
Table 5 Comparison of the electrochemical parameters for OER derived from electrochemical impedance spectroscopy at the surfaces of Ni foam baseline material modified with different catalysts, under alkaline conditions..... 40
Table 6 Total, average values of charge-transfer resistance and double-layer capacitance parameters, obtained for a single-cell electrolyser unit (anode: Ni foam; cathode: unmodified and Pd-supported Ni foam), recorded in 8.0 M KOH solution at 45 ºC..... 43
Table 7 Total, average values of the reaction resistance and double-layer capacitance parameters, obtained for a single-cell electrolyser unit (anode: electrooxidized or Co-modified Ni foam; cathode: Ir-activated Ni foam), recorded in 8.0 M KOH solution at 45 ºC. 46
Table 8 Chromatograhpic analysis of H_2 and O_2 gas samples generated during the continuous operation of 500 W AWE stack. 50

List of Abbreviations and Symbols

1. AWE – Alkaline Water Electrolysis
2. C_{Ads} – adsorption pseudocapacitance
3. C_{dl} – double-layer capacitance
4. CV – Cyclic Voltammetry
5. CVD – Chemical Vapour Deposition
6. EDX – Energy-Dispersive X-Ray Spectroscopy
7. EI – Electrochemical Interface
8. EIS – Electrochemical Impedance Spectroscopy
9. FRA – Frequency Response Analyzer
10. GC – Gas Chromatography
11. GHG – Greenhouse Gases
12. HER – Hydrogen Evolution Reaction
13. j_0 – exchange current-density
14. OER – Oxygen Evolution Reaction
15. OH_{Ads} – adsorbed hydroxyl species
16. PEM – Proton Exchange Membrane
17. R_{Ads} – adsorption charge-transfer resistance
18. R_{ct} – charge-transfer resistance
19. RES – Renewable Energy Sources
20. RHE – Reversible Hydrogen Electrode
21. SEM – Scanning Electron Microscopy
22. UV – Ultraviolet

Monothematic List of Publications as the Basis for the Ph.D. Thesis

I. **Mateusz Łuba**, Tomasz Mikołajczyk, Bogusław Pierożyński. Hydrogen Evolution Reaction on Iridium-Modified Nickel Foam Surfaces, *Electrocatalysis,* 2020, **11**, 347-353. **IF=2.743**

II. Bogusław Pierożyński, Tomasz Mikołajczyk, **Mateusz Łuba**, Alireza Zolfaghari. Kinetics of oxygen evolution reaction on nickel foam and platinum-modified nickel foam materials in alkaline solution. *Journal of Electroanalytical Chemistry*, 2019, **847**, 1-8. **IF=4.464**

III. **Mateusz Łuba**, Tomasz Mikołajczyk, Mateusz Kuczyński, Bogusław Pierożyński, Ireneusz M. Kowalski. Enhancing the Effectiveness of Oxygen Evolution Reaction by Electrodeposition of Transition Metal Nanoparticles on Nickel Foam Material, *Catalysts*, 2021, **11**, 1-13. **IF=4.146**

IV. Bogusław Pierożyński, Tomasz Mikołajczyk, Bogusław Wojciechowski, **Mateusz Łuba**. An Innovative 500 W Alkaline Water Electrolyser System for the Production of Ultra-Pure Hydrogen and Oxygen Gases. *Energies,* 2021, **14**, 1-11. **IF=3.004**

Scientific Achievements

List of other publications in scientific journals (7×)

1. Tomasz Mikołajczyk, **Mateusz Łuba**, Bogusław Pierożyński, Ireneusz M. Kowalski, Wiesław Wiczkowski, The Influence of Solution pH on the Kinetics of Resorcinol Electrooxidation (Degradation) on Polycrystalline Platinum, *Molecules*, 2019, **24**, 1-11.
2. **Mateusz Łuba**, Tomasz Mikołajczyk, Bogusław Pierożyński, Comparison of the Corrosion Resistance of Commercial coated steel and hot-dip Zn Coatings under Changing Environmental Conditions, *International Journal of Electrochemical Science*, 2019, **14**, 10306-10317.
3. Tomasz Mikołajczyk, **Mateusz Łuba**, Bogusław Pierożyński, Lech Smoczyński, A Detrimental Effect of Acetonitrile on the Kinetics of Underpotentially Deposited Hydrogen and Hydrogen Evolution Reaction, Examined on Pt Electrode in H_2SO_4 and NaOH Solutions, *Catalysts*, 2020, **10**, 1-13.
4. **Mateusz Łuba**, Tomasz Mikołajczyk, Bogusław Pierożyński, Lech Smoczyński, Paweł Wojtacha, Mateusz Kuczyński, Electrochemical Degradation of Industrial Dyes in Wastewater through the Dissolution of Aluminum Sacrificial Anode of Cu/Al Macro-Corrosion Galvanic Cell, *Molecules*, 2020, **25**, 1-17.
5. Bogusław Pierożyński, Tomasz Mikołajczyk, **Mateusz Łuba**, Paweł Wojtacha, Lech Smoczyński, Acetonitrile's Effect on the Efficiency of Ethanol Electrooxidation at a Polycrystalline Pt Electrode in Relation to pH-Dependent Fuel Cell Applications, *Catalysts*, 2020, **10**, 1-16.
6. Mateusz Kuczyński, **Mateusz Łuba**, Tomasz Mikołajczyk, Bogusław Pierożyński, Agnieszka Jasiecka-Mikołajczyk, Lech Smoczyński, Piotr Sołowiej, Paweł Wojtacha, Electrodegradation of Acid Mixture Dye through the Employment of

Cu/Fe Macro-Corrosion Galvanic Cell in Na_2SO_4 Synthetic Wastewater, *Molecules*, 2021, **26**, 1-15.

7. Mateusz Kuczyński, **Mateusz Łuba**, Tomasz Mikołajczyk, Bogusław Pierożyński, The Effect of Resorcinol on the Kinetics of Underpotentially Deposited Hydrogen and the Oxygen Evolution Reaction, Studied on Polycrystalline Pt in a 0.5 M H_2SO_4 Solution, *Energies*, 2022, **15**, 1-9.

Scientific Conferences:

1. **ŁUBA, M.** Reakcja wydzielania wodoru na piance niklowej zmodyfikowanej molibdenem oraz kobaltem. Problemy w inżynierii mechanicznej, University of Warmia and Mazury in Olsztyn, Olsztyn, Poland, 26-28 June 2019.
2. **ŁUBA, M.** Hydrogen evolution at iridium-modified nickel foam catalyst. 20th International Conference – Advanced Batteries, Accumulators and Fuel Cells, Brno University of Technology, Brno, 6-9 August 2019.
3. **ŁUBA, M.;** KUCZYŃSKI, M. Hydrogen Evolution Reaction on CoMo- and MoNi-alloy Modified Nickel Foam Surface, Hydrogen Days 2021 – 11th International Conference on Hydrogen Technologies, University of Chemistry and Technology in Prague, Prague, 24-25 March 2021.
4. **ŁUBA, M.;** KUCZYŃSKI, M. Electrochemical Removal of Dye-based Industrial Wastewater Through the Electrocoagulation with Fe ions derived from Cu/Fe Macro-corrosion Galvanic Cell, 2nd International Conference on Water Management and its Surroundings – Theoretical and Practical Aspects, University of Warmia and Mazury in Olsztyn, Olsztyn, Poland, 20-21 May 2021.

External Internship:

1. Scientific internship at University of Chemistry and Technology in Prague (Czech Republic), within the period of July 26th to August 26th, 2021.

Bibliometric Data (Scopus):

1. Publications in scientific journals: 11
2. Citations by 27 documents
3. H-index: 3
4. Total Impact Factor: 40.708
5. Total MNiSW points (2019): 1100

Acknowledgments

Mateusz Łuba participated in the Interdisciplinary Doctoral Studies in Bioeconomy (POWR.03.02.00-00-1034/16-00), funded by the European Social Fund.